*Annual Review of Earth and Planetary Sciences*

# Permeability of Clays and Shales

C.E. Neuzil

US Geological Survey, Reston, Virginia 20192, USA; email: ceneuzil@usgs.gov



Annu. Rev. Earth Planet. Sci. 2019. 47:247–73

The *Annual Review of Earth and Planetary Sciences* is online at earth.annualreviews.org

https://doi.org/10.1146/annurev-earth-053018-060437



**Keywords**

permeability, hydraulic conductivity, clay, mudrock, shale

**Abstract**

The low permeability of clays, shales, and other argillaceous lithologies makes them key controls of transport and deformation processes in the crust but is known for being challenging to characterize. As muds are modified by compaction and diagenesis to low-porosity shales, permeability can decrease by six or more orders of magnitude, but at large scales it is often dramatically and unpredictably increased by fractures, faults, and other features. Testing and inverse modeling show that petrophysical properties and the geological environment are dominant controls of clay and shale matrix permeability and its scale dependence. Active sedimentation and tectonism on continental margins cause large-scale permeability to vary with time, but in stable continent interiors it is unclear how regional permeability of argillaceous formations changes over time or, in most cases, what controls it. Although rarely considered, it is also unknown whether Darcian permeability adequately describes flow in clay-rich materials.

- Critical for problems in energy, water supply, waste isolation, and geologic hazards, clay and shale permeability remains problematic.
- Test data and inverse model analyses are beginning to reveal where and how permeability of clay and shale changes with scale.
- In clays and shales, causes of permeability scale effects, their time dependence, and even flow behavior continue to raise questions.

## 1. INTRODUCTION

**Clay:** an aggregate of fine (typically <2 μm) sediment with phyllosilicate (clay) minerals usually dominant; also phyllosilicate minerals themselves

**Argillaceous:** containing significant clay, here lithologies with 20% or more by weight

Abundant, widely distributed, and among the least permeable of geologic materials, clays, shales, and other argillaceous lithologies (see the sidebar titled Argillaceous Sediments and Sedimentary Rocks) are critical controls of fluid flow, mass and heat transport, and mechanical behavior in the upper crust (**Figure 1**). They are best known for delimiting flow in more permeable lithologies, such as confining aquifers and protecting them from contamination (Bredehoeft et al. 1983, Parker et al. 2004), blocking upward migration of injected chemical wastes and $CO_2$ (Brasier & Kobelski 1996, Intergov. Panel Clim. Change 2005), trapping oil and gas in reservoir rocks (Best & Katsube 1995), capping overpressured reservoirs (Fertl 1976), and limiting exchange of fluids and heat between oceans and underlying oceanic crust (Spinelli et al. 2004). Clay and shale formations themselves can be such isolated environments that attention is now focused on some for hosting nuclear waste (Neuzil 2013) and on others because of their largely untapped oil and gas resources (US Energy Inf. Admin. 2015). Difficulty expelling water from argillaceous sediments as they are buried or tectonically compressed keeps them mechanically weak. Among other things, this can control faulting and seismicity (Mase & Smith 1987, Saffer & Bekins 2006), submarine slope failure (Dugan & Flemings 2000), and land subsidence (Ingebritsen et al. 2006), and it also causes soft-sediment shale tectonics, including mud diapirs and mud volcanoes (Wood 2010).

The permeability of clays, shales, and other clay-rich lithologies—the measure of their ability to transmit fluids (see the sidebar titled Darcy's Law, Permeability, and Hydraulic Conductivity)—is consequently a crucial parameter in many scientific and engineering applications, but it has long been recognized as challenging to characterize. It is small enough that measurements require special techniques (Schlömer & Krooss 1997) and cannot replicate flow conditions in the subsurface (Neuzil 1986, Dixon et al. 1999). This historically limited the number of permeability measurements in argillaceous materials and has left unanswered fundamental questions about how to describe flow in them (Mitchell 1993, Liu et al. 2012). The most troublesome limitation researchers and analysts face, however, may be that of scale. Low-permeability measurement can be done only on scales that are much smaller than most applications. This is particularly problematic for argillaceous formations because faults, fractures, or other features often increase their effective permeability by orders of magnitude (van der Kamp 2001) but are difficult to detect or predict (Bredehoeft et al. 1983, Mase & Smith 1987).

Growing focus on clays and shales in several fields has expanded efforts to measure and otherwise characterize their permeability, often in environments that previously saw little study. Scientific ocean drilling and, more recently, nuclear waste repository programs have joined water resource and contamination studies, geotechnical engineering efforts, and oil and gas industry research as important sources of permeability data. Here I examine what test data and other evidence

### ARGILLACEOUS SEDIMENTS AND SEDIMENTARY ROCKS

The phrase clay and shale is used here as shorthand for a range of argillaceous sediments and sedimentary rocks that includes muds, clays, mudstones, marls (containing significant fine-grained carbonates), siliceous mudstones (containing significant fine-grained silica), shales, and argillites in rough order of progressing compaction and diagenesis. Terminology and definitions for these lithologies are erratic (Potter et al. 2005). In North America, the term shale is often applied to all but muds, soft clays, and marls, although it is sometimes restricted to lithologies that part along bedding planes. The terms mudrock, mudstone, claystone, and argillite are in most routine use outside North America.

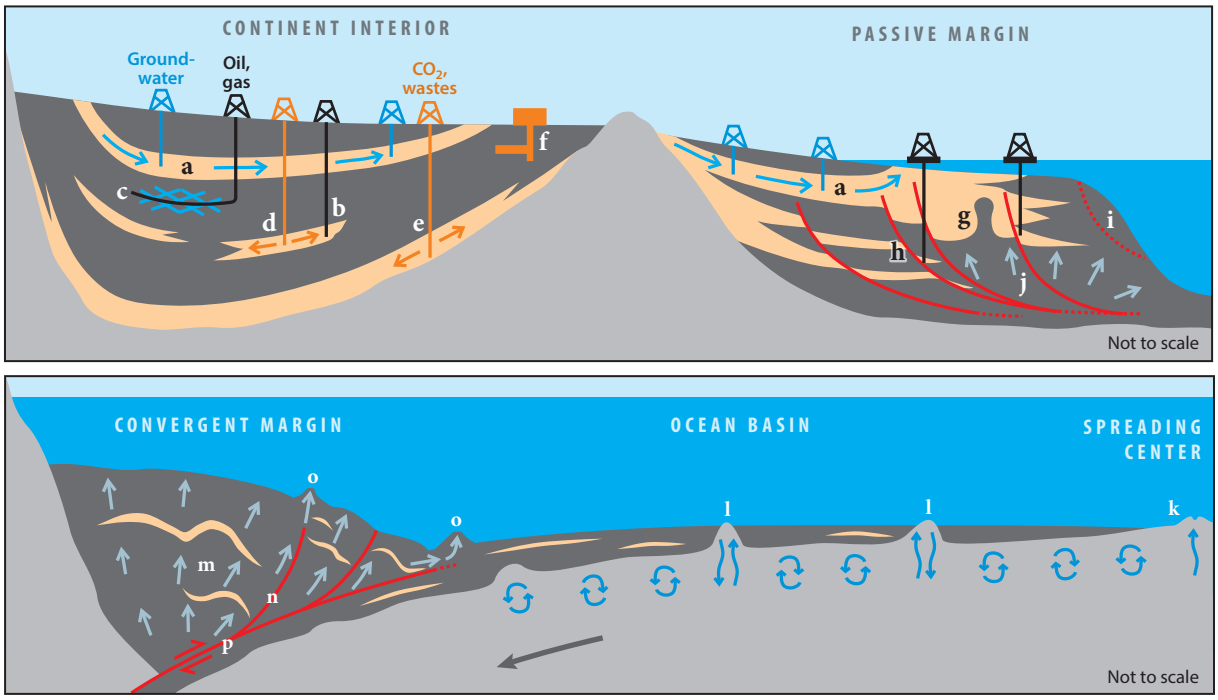


**Figure 1**

Schematic cross sections illustrating the role of low-permeability clays and shales in human activities, geologic hazards, and crustal processes. (*Top*) Regional groundwater flow systems in continent interiors and passive margins (*a*) are widely used sources of groundwater (*blue wells*) created by argillaceous confining strata, which also protect aquifers from surface and subsurface contamination. Deeper shales cap conventional oil and gas reservoirs (*b*), and some are themselves important sources of unconventional oil and gas when hydrofractured (*c*) (both: *black wells*). $CO_2$ injected to enhance oil recovery (*d*) or sequestered in saline aquifers is confined by shale cap rocks, as are injected chemical wastes (*e*) (both: *orange wells*). Shales and clay rocks are also expected to isolate some spent nuclear fuel (*f*). Passive margins have active sedimentation, and difficulty expelling pore fluid from clay-rich muds raises fluid pressures and delays compaction, keeping the muds soft and resulting in shale diapirism (*g*), gravity-driven shale-tectonic faulting that creates structural traps for oil and gas (*h*), and potentially tsunami-genic submarine slope failures (*i*); elevated pore fluid pressures also pose blowout hazards when drilling (*j*). (*Bottom*) Oceanic crust accumulates fine-grained, often clay-rich sediment as it moves away from spreading centers over time. Where the crust is young and sediment is thin or absent, hot fluids in the crust are able to vent to the ocean (*k*). As sediment thickness increases away from spreading centers, exchange of water, heat, and chemical mass with the ocean is focused at seafloor outcrops (*l*). At convergent margins voluminous clay-rich accretionary prisms (*m*) can form as sediment is scraped from subducting oceanic crust. Here too, difficulty expelling water results in high pore fluid pressures, keeping sediments weak and, among other things, enabling thrust faulting (*n*) and mud volcanoes (*o*). The high pressures also mediate slip along the décollement, or faults between subducting and accreting sediment (*p*), that results in many of the world's most destructive earthquakes and tsunamis.

## DARCY'S LAW, PERMEABILITY, AND HYDRAULIC CONDUCTIVITY

Flow through most porous materials is well described by a constitutive relation known as Darcy's law. If fluid density does not vary greatly, it can be expressed simply as

$$q = -\frac{k\rho g}{\mu}\nabla h,$$

indicating that fluid flux per area $q$ (length/time) is proportional to the hydraulic driving force denoted as a gradient in fluid potential or head $h$ (length). Permeability $k$ (length$^2$) is defined by Darcy's law and controlled by pore size and tortuosity, or irregularity, of paths fluid takes through the pores. The quantity $k\rho g/\mu$ is hydraulic conductivity $K$ (length/time), which includes fluid density $\rho$ (mass/length$^3$) and viscosity $\mu$ (mass/length time), as well as $g$ (length/time$^2$). For aqueous fluids at room temperature, $\rho g/\mu$ is approximately $10^7$ m$^{-1}$ s$^{-1}$. At 5-km depth, $\rho g/\mu$ is approximately $5 \times 10^7$ m$^{-1}$ s$^{-1}$ largely because $\mu$ decreases with temperature. Measured $k$ in geologic materials spans a mind-boggling 17 orders of magnitude, from about $10^{-24}$ to $10^{-7}$ m$^2$, with measured values for clays and shales usually falling between about $10^{-23}$ and $10^{-15}$ m$^2$.

currently reveal about clay and shale permeability, how it depends on the scale considered, and how it may vary with time in different geological settings. In the process I highlight certain stubborn gaps in understanding that may be important areas for future research.

I lay the groundwork for this review in Section 2, which surveys low-permeability testing techniques, their limitations, and the data they have provided. Laboratory tests have contributed the vast majority of permeability data for argillaceous lithologies and show how lithology, compaction and diagenesis, and geologic environment influence the small-scale or matrix permeability of clays and shales. Matrix permeability controls transport to and from fluid-conducting faults and fractures as well as large-scale behavior when such features are absent. Borehole testing, which offers clues to where and how faults and fractures increase permeability, is also considered. Section 3 examines large-scale clay and shale permeability data obtained from inverse flow modeling and the scale effects revealed when they are compared with test data. Anomalously pressured systems ranging from accretionary complexes to shallow intraplate formations allow particularly definitive analyses, but a largely untapped source of large-scale clay and shale permeability data also exists as a by-product of regional groundwater flow studies. Dynamic, or time-dependent, permeability emerges as an important aspect of large-scale permeability. Section 4 considers clay and shale permeability in the broader context of permeability in the crust, and Section 5 summarizes current understanding and assesses needs for future research. Conspicuous uncertainties surround the causes of scale effects in certain environments, their time-dependent or dynamic nature, and, perhaps surprisingly, fundamental laws governing flow in argillaceous materials.

## 2. PERMEABILITY OF CLAY AND SHALE FROM TESTS

**Matrix permeability:** permeability due to intergranular pores without secondary pathways such as fractures

Permeability testing generally requires controlling or altering flow in the tested material. In low-permeability lithologies there are extreme limitations on the scale of tests because of the time required to accomplish this (Neuzil 1986, Mase & Smith 1987). Test duration increases with the square of length tested, and practical durations of days to weeks limit sample dimensions in most argillaceous lithologies to less than a meter and generally to centimeters or less. In situ tests are similarly limited, with borehole tests, for example, characterizing only a narrow zone adjoining the borehole. While limiting in most respects, small sample sizes have also had the beneficial side

effect of allowing spatially variable properties such as porosity and clay content to be characterized relatively unambiguously, clarifying how they influence permeability.

### 2.1. How Low Permeability Is Measured

Low-permeability tests have come into wide use but remain demanding to implement, especially at the lowest permeabilities (Best & Katsube 1995, Boulin et al. 2010). Conditions in tests also invariably differ from in situ conditions and potentially introduce artifacts. Hydraulic gradients are a conspicuous example. It is possible in principle to use arbitrarily large hydraulic gradients to produce fluid fluxes large enough to measure easily (see the sidebar titled Darcy's Law, Permeability, and Hydraulic Conductivity), but in practice hydraulic gradients must be minimized to reduce mechanical disruption of the sample (Schlömer & Krooss 1997) and to avoid leaks and other problems in test equipment that high fluid pressures can cause. Difficulty controlling and measuring small fluid fluxes, however, limits how much hydraulic gradients can be reduced (Schlömer & Krooss 1997). As a result, low-permeability tests compromise between the low extreme of fluid flux measurement and higher-than-desired hydraulic gradients.

Reported test protocols reveal that the practical lower limit for fluid flux in laboratory tests is in the neighborhood of $10^{-9}$ mL $s^{-1}$ (Neuzil 1986, Dixon et al. 1999). For most clays and shales, achieving this requires hydraulic gradients of 1 to in excess of $10^3$, while gradients in the subsurface are typically less than $10^{-1}$. This distinguishes low-permeability geologic materials as having no experimental observations of flow under typical in situ conditions. The applicability of Darcy's law in these conditions is thus an assumption, and it is one that some researchers have questioned (see the sidebar titled Non-Darcian and Coupled Flow in Argillaceous Materials).

Sample and formation damage are of particular concern in testing because they can significantly affect low-permeability materials. Stress release and drying of cores, for example, often cause microfractures that can be difficult to detect (e.g., Neuzil 1993). Damage and apparatus leaks are probably the most common test problems and tend to inflate measured permeabilities. Because of this, overestimation of low permeability is the presumptive bias, and reported values for clays and shales should generally be treated as maxima. However, erroneously small values are occasionally suspected from incomplete sample saturation, microbial growth and colloidal clogging, chemical

#### NON-DARCIAN AND COUPLED FLOW IN ARGILLACEOUS MATERIALS

Because experiments in clays and shales occasionally show unexplained deviations from Darcy's law, its applicability to these materials has been questioned for decades (e.g., Mitchell 1993, Liu et al. 2012). Altered water properties near clay mineral surfaces in micro- to nanometer-size pores are often suggested as the cause, with non-Newtonian behavior, for example, reducing or stopping flow under low hydraulic gradients (e.g., Dixon et al. 1999, Liu et al. 2012). This is a thorny issue because several types of experimental artifacts have been implicated in giving the appearance of non-Darcian behavior, including flux or hydraulic gradient measurement errors, sample deformation, microbial growth, gas generation, and colloidal clogging (Neuzil 1986, Mitchell 1993). Coupled flows further complicate matters. Coupled flows include fluid flow driven by gradients in solute concentration and electrical potential—chemical and electro-osmosis—and are well documented in natural argillaceous materials (Neuzil & Provost 2009). A particular difficulty lies in the fact that flow in clays can actually create such gradients; electrical potential gradients generated this way, for example, are called streaming potentials and are suspected as the cause of some reported non-Darcian behavior (Neuzil 1986).

reactions, and volume changes in clay minerals exposed to non-native permeants (Mesri & Olson 1971, Dixon et al. 1999).

Approaches to measuring clay and shale permeability include simple steady-flow tests (Schlömer & Krooss 1997, Zhang et al. 2002), but methods that are devised specifically for low-permeability materials and that rely on surrogates for fluid flow measurement are more common (**Figure 2**). The latter include pressure-pulse tests where flow is calculated from pressure changes in a closed reservoir or borehole (e.g., Lecampion et al. 2006, Giot et al. 2014, Beauheim et al. 2014) and consolidation and constant strain rate tests that use deformation to track flow into or out of a sample (Mitchell 1993, Katsuki et al. 2014). A deformation test introduced by Zhang & Scherer (2012) illustrates the effort that can be expended to measure especially small

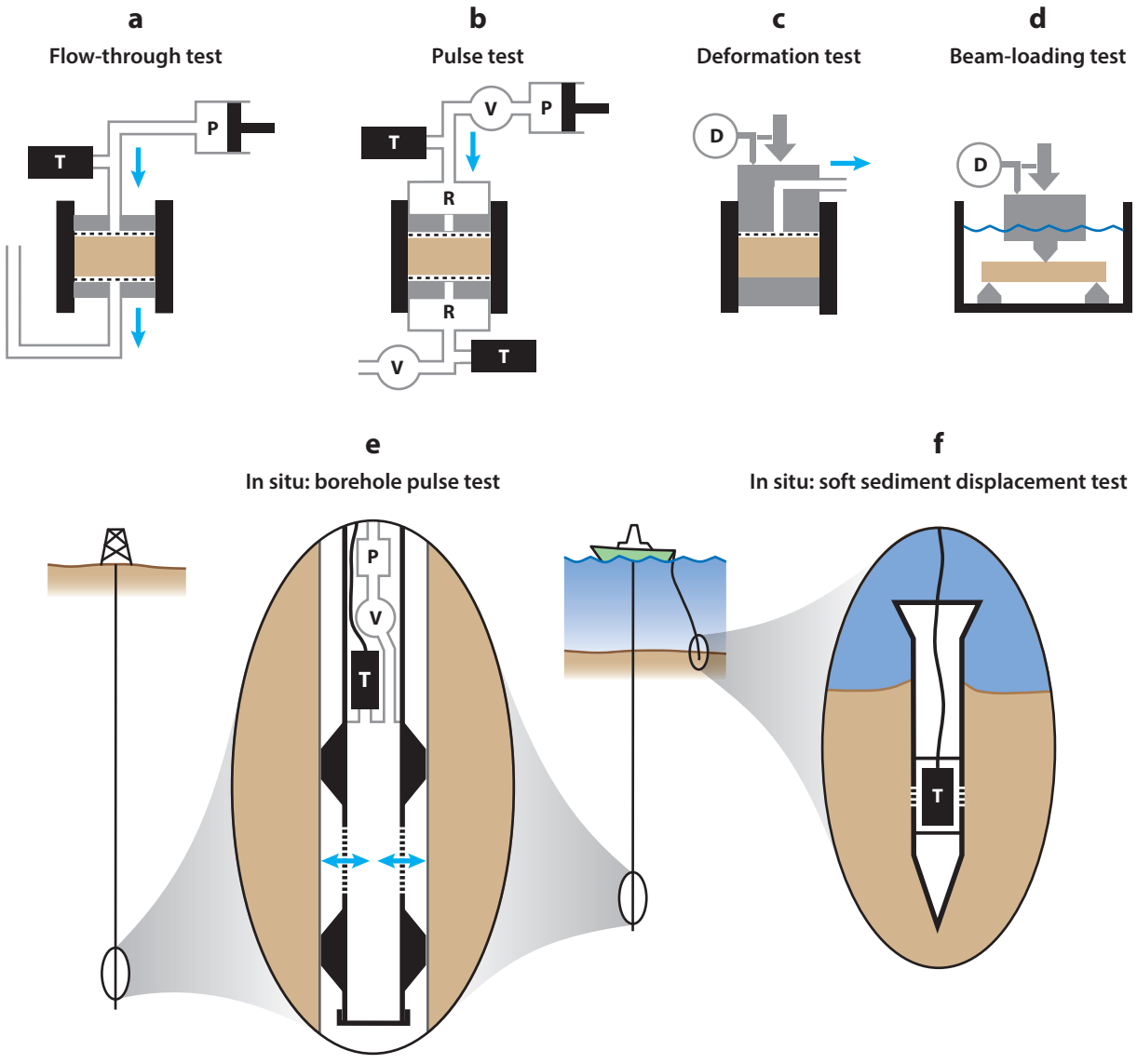


(*Caption appears on following page*)

**Figure 2** (*Figure appears on preceding page*)

Approaches used to measure the permeability of clays, shales, and muds. Test apparatuses are shown considerably simplified to convey the essence of each technique. Flow-through tests (*a*) require generating measurable flow through the sample that is used with the applied pressure difference to determine permeability once a steady state is reached. Pulse tests (*b*) typically apply a sudden pressure increase in the upstream reservoir that is then shut in with a valve; decay of the pressure pulse and increasing pressure in the downstream reservoir together with fluid and reservoir compressibility values are used to calculate the fluid fluxes and permeability. Deformation tests include consolidation and constant rate of strain tests. The former track compaction under an abrupt increase in load while the latter track the load required for compaction at a constant rate; both (*c*) are controlled by the rate of pore fluid expulsion, which can be related to permeability. Likewise, the relatively new beam-loading technique tracks bending of a step-loaded shale prism (*d*) as pore fluid redistributes within the shale and exchanges with the surrounding bath. In situ tests (*e*,*f*) include variants of laboratory pulse and deformation techniques. Commonly used borehole pulse tests (*e*) analyze the decay of a fluid pressure pulse shut in between packers. Dropped probes that penetrate soft sediment on the ocean floor (*f*) track decay of the fluid pressure increase caused by the rapid compaction of sediment displaced by the probe. The various approaches have different limitations that dictate how they can be applied. Consolidation and constant rate of strain tests, for example, work best for relatively deformable samples, while the beam-loading test can be used only with well-compacted and lithified shales. Abbreviations: D, displacement or load sensor; P, pump; R, fluid reservoir; T, pressure transducer or other pressure-measuring device; V, valve.



permeabilities and involves monitoring deformation of a machined shale beam when a load is applied to it. Zhang & Scherer used the technique to determine a permeability below $10^{-23}$ m$^2$, the lowest well-documented value I know.

In situ tests are usually pressure-pulse procedures in boreholes shut in with packers, although constant fluid injection or withdrawal at small rates (Vinsot et al. 2011), long-term pressure evolution (Neuzil 1993), analysis of responses to tidal and other mechanical loads (van der Kamp 2001), and pressure responses to probe insertion in soft marine sediment (Davis et al. 1991), among others, also see use. These approaches bring their own challenges. In borehole tests, for example, extreme care is required to rule out leaks and equipment malfunctions downhole (Beauheim et al. 2014), and boreholes can be affected by instability, deformation, and failure of the formation (Neuzil 1993, Winkler 2005, Bekins et al. 2011), as well as thermal perturbations and drilling damage (Pickens et al. 1987). Borehole tests have nevertheless apparently succeeded in measuring permeabilities on the order of $10^{-23}$ m$^2$ (Beauheim et al. 2014) or nearly as small as laboratory tests.

## 2.2. Permeability Data from Laboratory Tests

Laboratory test data reveal how profoundly compaction and diagenesis alter argillaceous sediments; as these processes reduce porosity from about 0.8 in newly deposited muds to less than 0.1 in shales, matrix permeability generally decreases by six or more orders of magnitude (**Figure 3**). **Figure 3** shows compiled permeability-porosity data for argillaceous sediments and rocks from tests believed reliable based on test description and for which clay fraction and geologic environment are reported. Refined clays, resedimented or remolded samples, and lithologies with less than 20% clay were excluded. Permeabilities obtained using gas and nonaqueous fluids and from unsaturated samples also were not used because both drying and permeants such as liquid organics alter pore structure and cause other changes that can affect permeability in clay aggregates (Mitchell 1993, Anandarajah 2003). At porosities above about 0.3, these criteria were met by a large number of data derived largely from scientific ocean drilling on convergent and passive continental margins. Fewer data were located for lower porosities and are mostly from nuclear repository programs, oil and gas industry research, geotechnical analyses, and groundwater resource studies in a mix of on- and offshore environments.

Peculiarities of available clay and shale permeability data should be borne in mind when interpreting **Figure 3**. Nearly all permeabilities are normal to bedding, but in a few instances only bedding-parallel values were available and are included. Clay and shale permeability is anisotropic,

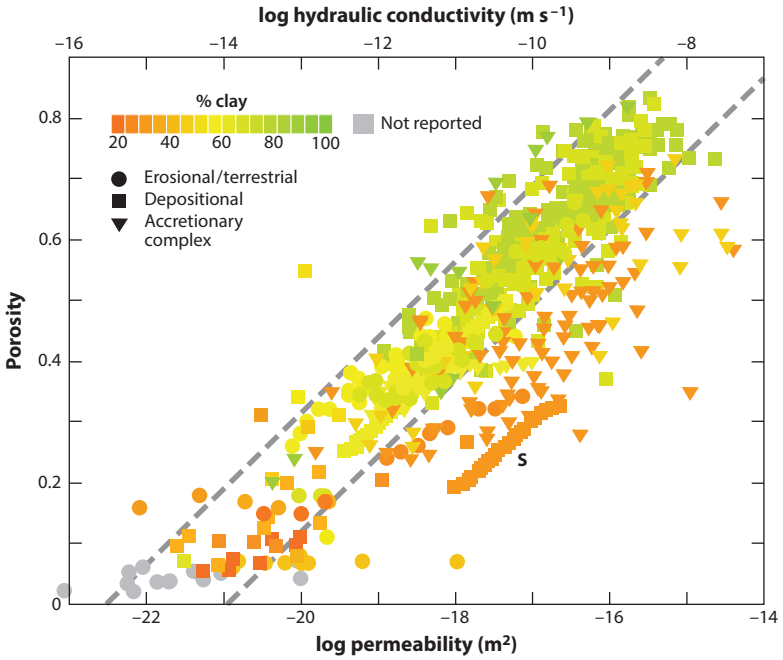


**Figure 3**

Matrix permeability of clay and shale from laboratory tests plotted versus porosity and showing clay fraction and geologic setting. The hydraulic conductivity scale is for aqueous fluids at room temperature. Data are from Horsrud et al. (1998), Dewhurst et al. (1999), Bryant (2002), Croisé et al. (2004), Heitzmann (2004), Kwon et al. (2004), Boisson (2005), Delay et al. (2006), Ota et al. (2007), Yang & Aplin (2007), Yven et al. (2007), Kitajima et al. (2012), Reece et al. (2012), Zhang & Scherer (2012), Yu et al. (2013), Daigle & Screaton (2015), and Bossart et al. (2017). Data from Zhang & Scherer (2012) with unreported clay contents are included to show the full range of measured values. To emulate a 2-μm-grain-size threshold for sedimentologically defined clay, clay fractions of data from Daigle & Screaton (2015) are shown as 70% of the reported values, which were based on a 4-μm threshold. Dashed gray lines indicate permeability maxima and minima defined by Equation 1 as discussed in the text. S indicates data from a formation described as a siltstone.

with bedding-parallel values often 1.5 to 5 times larger than bedding-normal values in laboratory samples (Clennell et al. 1999), due partly to bedding-parallel alignment of platelet-shaped clay grains. However, anisotropy values exceeding 10 have been noted in samples with thin but highly heterogeneous stratification or that have been subjected to shear deformation (Daigle & Screaton 2015).

The plot also intermingles different definitions and measurement techniques for both porosity and clay fraction. Total rather than effective, accessible, or liquid porosity was used because it is the only value reported for many data. Total porosity includes pore space not contributing to flow, including interlayer water in clay minerals. Gamage et al. (2011) concluded that when using total porosity in plots like **Figure 3**, the apparent permeability trend is one to two orders of magnitude too low at total porosity values below 0.2. Subtracting interlayer water for smectite contents of 30–50% yields effective porosities some 10–15% smaller than total porosities; this shifts data down in **Figure 3**, resulting in a trend indicating higher permeabilities at low porosities. For characterizing clay content, most clay fractions are by weight based on sedimentological size class, but a few

used X-ray diffraction data or optical counts and presumably are by volume. Sedimentologically defined clay fractions, moreover, include varying but usually small amounts of nonclay minerals as well as different mixes of clay minerals, both of which can influence permeability (Mesri & Olson 1971).

Mechanisms by which compaction and clay fraction control matrix permeability in sediments have been examined by several researchers, including Koltermann & Gorelick (1995), Revil et al. (2002), Yang & Aplin (2010), Schneider et al. (2011), and Luijendijk & Gleeson (2015). Koltermann & Gorelick (1995) and Revil et al. (2002) noted that permeability and porosity should be minimized when clay is just sufficient to fill voids between larger nonclay grains that are in contact, which occurs at clay fractions of about 0.2 to 0.4. Luijendijk & Gleeson (2015) found that while artificial sand-clay mixtures did reach minimum permeabilities at clay contents of about 0.2, natural mixes of a range of sediment sizes showed more complex behavior. In **Figure 3**, lithologies with clay fractions of 0.2 to 0.4 tend to be more permeable than those with more clay at porosities larger than about 0.2. Schneider et al. (2011) suggested that permeability losses by compaction are minimized at low clay fractions by mechanical support of nonclay grains in contact. For lithologies with clay fractions below about 0.4 and porosities above about 0.2 in **Figure 3**, permeability does show a less systematic decrease with porosity than lithologies with higher clay fractions, consistent with that prediction. Yang & Aplin (2010) observed trends similar to **Figure 3** in data from natural, resedimented, and refined clays compacted in the laboratory but reported lower permeabilities for clay fractions exceeding 0.6, including especially low values that Mesri & Olson (1971) obtained for pure smectite clay.

Mechanical compaction alone cannot account for behavior in **Figure 3** because there is an overall decrease in clay fraction with decreasing porosity. Above 0.5 porosity, clay fractions are often 70% or higher. Below 0.5 porosity, few clay fractions exceed 60%; below 0.2 porosity, few exceed 50%. Bourg (2015) noted a similar trend in a different suite of shales. This may reflect a particular role for diagenesis in argillaceous sediments. Bjørlykke (1998) suggested that it is difficult to reduce the porosity of clay aggregates below 0.2 to 0.5 by mechanical compaction alone. Lower porosities result from processes that include clay mineral transformations that precipitate quartz (Thyberg et al. 2010) and dissolution-precipitation of nonclay minerals already present. The lowest porosities in argillaceous lithologies may typically require substantial nonclay constituents as in **Figure 3**. Precipitation of nonclay minerals can block pores and lead to lower permeabilities than possible with clay minerals only (Katsube & Williamson 1994), but understanding the processes that determine the extent to which pore throats become blocked is currently regarded as a prominent challenge in geochemistry (Stack 2015).

The log-linear trend in **Figure 3** suggests relating permeability $k$ to porosity $n$ using (e.g., Bekins et al. 1995)

$$\log k = \gamma n + \log k_0, \qquad 1.$$

where $k_0$ is the extrapolated intercept at zero porosity. Most data in **Figure 3** fall in a region defined by $\gamma = 8.0$ with $\log k_0$ values of $-22.5$ and $-21.0$ for minima and maxima. Data outside this envelope are predominantly on the higher side and dominated by clay fractions below about 40%, with the most conspicuous outliers from a formation described as siltstone (Reece et al. 2012). It is tempting to explain the few high-value outliers with relatively large clay fractions as measurement errors. Conversely, because erroneously low values of permeability from tests are thought to be rare, it is unclear how to interpret the few low-value outliers that fall quite consistently within an order of magnitude of the minima delineated by Equation 1 in **Figure 3**. They may show occasional unusually low values, such as those noted in smectite clays (Mesri &

Olson 1971). The nature of these few data is of interest because flow across stratification is limited by the lowest permeability horizons.

The geological environment appears to have relatively little influence on matrix permeability. Presumably, data below 0.3 porosity are frequently from eroding terrains because they offer the easiest access to rocks that have been subjected to deep burial and significant diagenesis. Data above 0.3 porosity from continental margins and ocean basins represent sediments that are relatively young and affected mostly by mechanical compaction. Some sediments in **Figure 3** from accretionary complexes may have experienced significant shear deformation, but Kitajima et al. (2012) found effects of shear deformation on permeability normal to shearing to be modest compared to compaction.

## 2.3. Permeability from Borehole Tests

A few borehole data can be associated with relatively unambiguous porosity and clay fraction values, allowing direct comparison (noting they are bedding-parallel values) with laboratory data as shown in **Figure 4**. The borehole data shown represent in situ test data generally in that some show permeabilities significantly larger than matrix values while others do not. The latter include a low-porosity Paleozoic shale and a mildly compacted Cretaceous mudstone. Scale effects, however, are apparent in two Jurassic shales and, rather dramatically, in a high-porosity Miocene mudstone onshore and nonindurated Miocene mud in an accretionary complex.

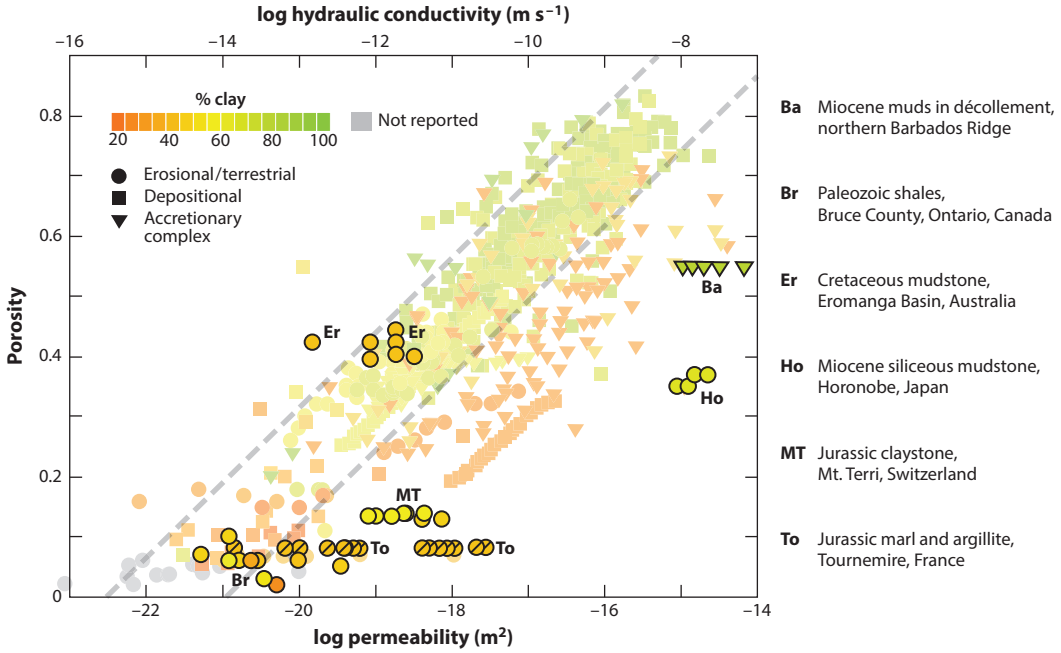


**Figure 4**

Permeability of clay and shale from borehole tests versus porosity as an overlay on laboratory test data. The hydraulic conductivity scale is for aqueous fluids at room temperature. Ba data are from Brown et al. (1994), Moore et al. (1995), Fisher & Zwart (1997), Zwart et al. (1997), and Bekins et al. (2011); Br data are from Walsh (2011), Roberts et al. (2011), and Intera Eng. Ltd. (2011); Er data are from Smerdon et al. (2014); Ho data are from Kurikame et al. (2008), Sanada et al. (2009), and Tachi et al. (2011); MT data are from Reisdorf et al. (2016) and Yu et al. (2017); and To data (*diagonal hash*) are from Boisson et al. (2001). The 70% clay fraction shown for Ho is by sedimentological size class, and the fraction of clay minerals is under 20%.

Bourg (2015) described evidence that formations with clay fractions below about 0.3 to 0.4 can maintain transmissive fractures, while fractures tend to close in formations with higher clay fractions. He suggested that the threshold is where nonclay grains come into contact, increasing unconfined compressive strength of the porous matrix, much like the mechanism Schneider et al. (2011) suggested limits compaction. Although clay fractions of the Jurassic shales are at or slightly above the threshold, this may explain the enhanced permeability in these formations, which evidence indicates is due to fractures (Boisson et al. 2001, Yu et al. 2017). The Paleozoic shale is also fractured, but its low permeability is maintained in part by halite and other mineral fracture fillings (Intera Eng. Ltd. 2011).

Data from the Barbados accretionary complex shown in **Figure 4** are from borehole pressure-pulse and constant flow tests that targeted the décollement, or faults, between accreting and subducting sediment. Although rich in clay, Miocene muds in the décollement also experience low effective stress that maintains relatively high permeability (Moore et al. 1995). The data spread resulted from testing at different fluid pressures and effective stresses, some of which resulted in hydrofractures because drilling-related deformation disturbed the local stress regime (Bekins et al. 2011). Natural flow along the décollement is thought to occur by such localized hydrofracturing (Brown et al. 1994) that migrates (Saffer 2015).

Fracture permeability in Miocene mudstone at Horonobe, Japan (Kurikame et al. 2008), at first appears exceptional because it has a clay fraction of about 0.7 (Tachi et al. 2011). However, the unit in question, the Wakkanai Formation, is a siliceous mudstone in which the fraction of mineralogical clay is less than 0.3 and so by Bourg's (2015) criterion is expected to maintain transmissive fractures. In this vein it should be noted that laboratory test data for the Wakkanai (Kurikame et al. 2008) are included in **Figure 3** and fall within the envelope in that plot.

## 3. CLAY AND SHALE PERMEABILITY BEYOND TEST SCALES

While in situ tests can reveal transmissive fractures and faults, as seen in **Figure 4**, they must be intersected by a borehole and little can be ascertained beyond the borehole's immediate vicinity. Fortunately, inverse model analysis permits characterizing clay and shale permeability at much larger scales. Inverse analysis uses known properties and modeled behavior of a system to constrain one or more unknown properties. Strictly speaking, most low-permeability tests are themselves inverse model analyses, but in their case they are applied to simple, well-defined systems under controlled conditions.

Inverse analyses are most readily used to characterize low permeability at large scales when applied to groundwater systems undisturbed by human activity; this essentially permits treating flow systems as long-running permeability tests, bypassing time limitations of human-managed procedures. Inverse model analysis has allowed characterizing the permeability of clay-rich sedimentary sequences up to several kilometers thick and hundreds of kilometers in lateral extent.

The trade-offs for this highly useful capability include uncertainty, the effort required for analysis, and limited applicability. Other aspects of the system and its behavior—for example, fluid head and permeability in aquifers, the geologic history, and system boundary conditions—must be sufficiently well understood to usefully constrain the permeability of argillaceous units. Some flow systems permit relatively well-posed analyses that yield large-scale clay or shale permeability with high confidence. However, as flow system complexity increases, nonuniqueness and uncertainty also grow and errors in conceptualizing the system become more likely (Bredehoeft 2005). Again invoking the analogy with permeability tests, developing a conceptual model is equivalent to inferring both the test procedure and how the test apparatus is constructed. Finally, not all systems lend themselves to inverse analysis. For example, analysis may be difficult or precluded in

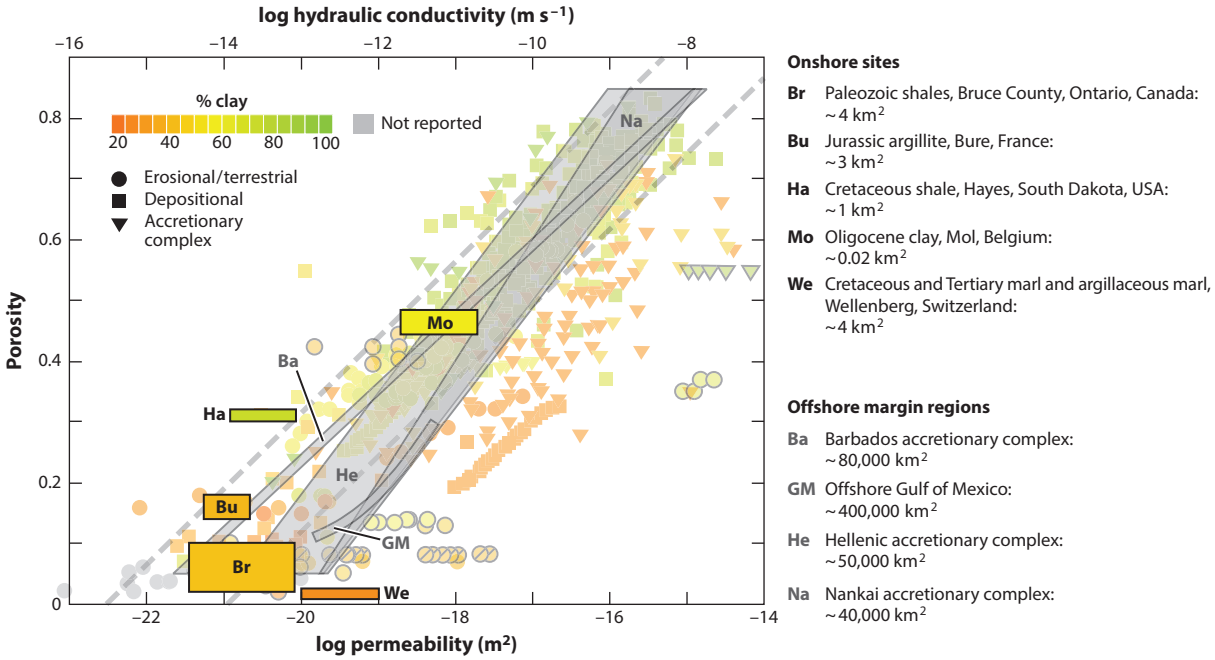


**Figure 5**

Site- and regional-scale permeability of clay and shale versus porosity as an overlay on laboratory and borehole test data. The hydraulic conductivity scale is for aqueous fluids at room temperature. Rectangles are ranges of porosity and permeability for onshore sites less than about 1 km deep (Neuzil 2015, and sources therein), and gray trends are regional values from offshore continent margins. Ba data are from Saffer & Bekins (1998), GM data are from Bethke (1986) and Harrison & Summa (1991), He data are from Kufner et al. (2014), and Na data are from Saffer & Bekins (1998).

groundwater systems that are especially complex, sparsely characterized, or significantly altered by human activity.

Like laboratory tests, inverse model analyses can be applied to both steady-state and transient flow systems. However, scenarios that have been used to obtain inverse estimates of large-scale clay and shale permeability are so diverse that further generalizations, including about reliability, are difficult. In each case, evaluation of the conceptual model and its assumptions must guide judgment. With these caveats noted, overall consistency in data from inverse analyses and comparison with other evidence suggests that they offer a useful perspective on clay and shale permeability not obtainable any other way (e.g., Saffer & Tobin 2011).

## 3.1. Large and Small Scales Compared

**Fluid potential:** also hydraulic head; a measure of potential and pressure energy of pore fluid

In a handful of instances, inverse analyses have yielded large-scale permeabilities linked to porosity and in some cases clay fraction, allowing direct comparison with laboratory-determined matrix permeabilities as shown in **Figure 5**. These large-scale data are almost entirely from presumed transient groundwater flow systems with pressure anomalies. Pressure anomalies are isolated subsurface minima or maxima in pore fluid potential indicating net inward or outward flow. Possible causes of the anomalies, including processes such as sediment compaction, tectonic deformation, and glaciation, are sufficiently slow or far enough in the past that the anomalies clearly delineate regions of low permeability (see the sidebar titled Fluid Pressure Anomalies and Permeability).

## FLUID PRESSURE ANOMALIES AND PERMEABILITY

A change in pore volume, fluid mass, or fluid density in a porous material also changes pore fluid pressure. Low-permeability formations can accumulate and maintain such pressure changes even when they are quite slow, just as car tires maintain inflation with infrequent topping up. Distinct pressure anomalies result when $|\Gamma| \geq K/l$ (Neuzil 1995), where $\Gamma$ (time$^{-1}$) is the forcing rate (the vigor of the change—for example, volume strain rate during tectonism), $K$ is hydraulic conductivity (length time$^{-1}$), and $l$ is the drainage length, or typically half the formation thickness. Surprisingly subtle geologic processes can cause pressure anomalies in clay and shale formations. For example, ongoing tectonism, compaction, or erosional decompaction often result in $\Gamma$ near $10^{-16}$ or $10^{-15}$ s$^{-1}$ (Neuzil 1995), which is sufficient for a distinct pressure anomaly in a 200-m-thick formation with a $K$ value of $10^{-14}$ or $10^{-13}$ m s$^{-1}$, respectively. Inverse analysis of pressure anomalies essentially involves determining $K$ from $\Gamma$ and $l$. Pressure anomalies also persist for some time after forcing ceases, and some attributed to past glaciation have provided constraints on permeability (e.g., Bekele 1999, Vinard et al. 2001).

Pressure anomalies have long been recognized in deep intracratonic basins, passive margins, and accretionary complexes (e.g., Fertl 1976, Westbrook & Smith 1983). Inverse analyses in these environments have been able to characterize how large-scale permeability likely varies with porosity in very thick sequences of compacting clay-rich sediments, with resulting trends for the Gulf of Mexico and the Barbados, Nankai, and Hellenic accretionary complexes (Bethke 1986, Bekins et al. 1995, Saffer & Bekins 1998, Kufner et al. 2014), as shown in **Figure 5**. Clay fraction is not shown for these data because the scales involved make it difficult to characterize. The volumes of clay-rich sediment represented are immense, with the sequences in question reaching thicknesses of several kilometers.

Continental margins are dynamic environments, often with vigorous sedimentary loading and tectonism deforming sediments and maintaining pressure anomalies (Saffer & Tobin 2011, Dugan & Sheahan 2012). The presence of pressure anomalies in relatively shallow clay and shale formations in stable intraplate settings is more surprising and only recently examined systematically (Neuzil 2013, 2015). **Figure 6** shows examples of pressure anomalies observed in two or more boreholes and also shows their estimated minimum extent. Studied under nuclear waste programs, the geological environments in **Figure 6** lack conspicuous processes to cause or maintain the anomalies. However, inverse model analyses invoking erosional decompaction, cycles of mechanical loading by glaciers, and terrain modification by erosion (Neuzil 1993, Vinard et al. 2001, Gonçalvès et al. 2004) can explain the anomalies using the permeability values for the sites shown in **Figure 5**.

The Mol, Belgium, site in **Figure 5** has no pressure anomaly but is included because extensive drilling and testing, including in an underground laboratory, give the large-scale permeability with reasonable confidence. Note that permeability at the Hayes, South Dakota, site is consistent with low outlier laboratory values. Shale there has a high percentage of smectite clay (Neuzil 1993) that, as noted in Section 2.2, exhibits particularly low permeability in laboratory tests.

Permeabilities in **Figure 5** apply over the anomalously pressured regions of the formations, ranging from thicknesses of tens to hundreds of meters at specific sites (**Figure 6**) to sequences several kilometers thick extending over areas on the order of $10^4$ to $10^5$ km$^2$. An absence of scale effects first noted by Neuzil (1994) is evident in **Figure 5**, and where clay fractions are available they are largely consistent with trends noted in laboratory test data. The apparent lack of scale effects in data from continental margins in that figure is remarkable not only because of the large volumes of sediment they represent but also because they are such geologically active

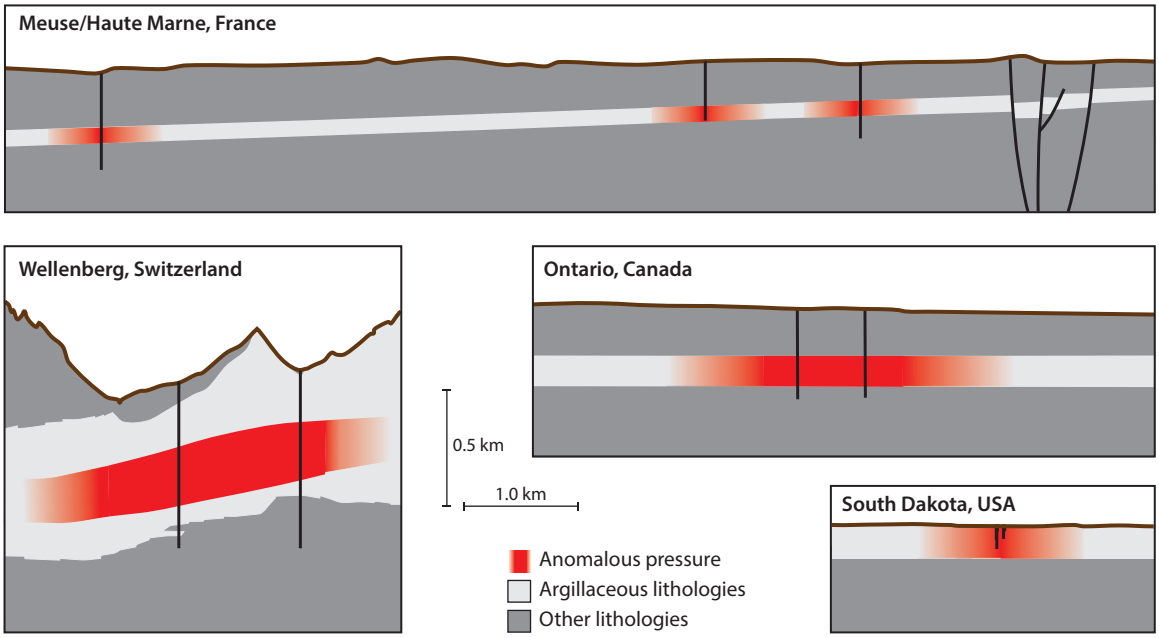


**Figure 6**

Pore fluid pressure anomalies in argillaceous formations in continent interiors. Depicted extents of anomalies are conservative extrapolations of pressure trends between boreholes, and actual extents could be much greater. In particular, the data are consistent with the presence of pervasive anomalous pressures in the Meuse/Haute Marne region of France. Fluid potentials at the latter sites are anomalously high (Gonçalvès et al. 2004), while they are anomalously low at the sites in Ontario (Intera Eng. Ltd. 2011), South Dakota (Neuzil 1993), and Wellenberg (Natl. Genoss. Lager. Radioakt. Abfälle 2002).

environments. Fluid pressures in these systems are typically near the least principal stress (Bethke 1986, Saffer & Tobin 2011), a sign that they are limited by sporadic natural hydrofracturing and rapid fluid expulsion. Lower permeability values presumably would prevail in the absence of high fluid pressures. The time-varying permeability of these systems is considered further in Section 3.3.

## 3.2. Large-Scale Permeability with Depth in Intraplate Settings

Much of available clay and shale permeability data from inverse analysis, and the majority for the largest scales, derive from systems in stable intraplate settings that are considered to be in long-established steady states. Inverse model analyses of steady-state flow systems are analogous to steady-state permeability tests. Groundwater flux across argillaceous units, and their system-wide permeability, is constrained by analyzing their influence on aquifer behavior. In a few instances, mass transport inferred from geochemical observations has provided additional constraints (Wei et al. 1990, Castro et al. 1998, Bethke et al. 1999).

Porosity and clay fraction of argillaceous units usually cannot be readily characterized in regional studies, so direct comparison with laboratory matrix permeabilities is not possible. However, it is informative to consider permeabilities from inverse analyses across a range of scales with depth as shown in **Figure 7**. Because the upper kilometer of the crust is important for many human activities, a logarithmic depth scale is used to display it clearly. Vertical and horizontal extents of regions in the plot indicate the range in formation depth and estimated permeability.

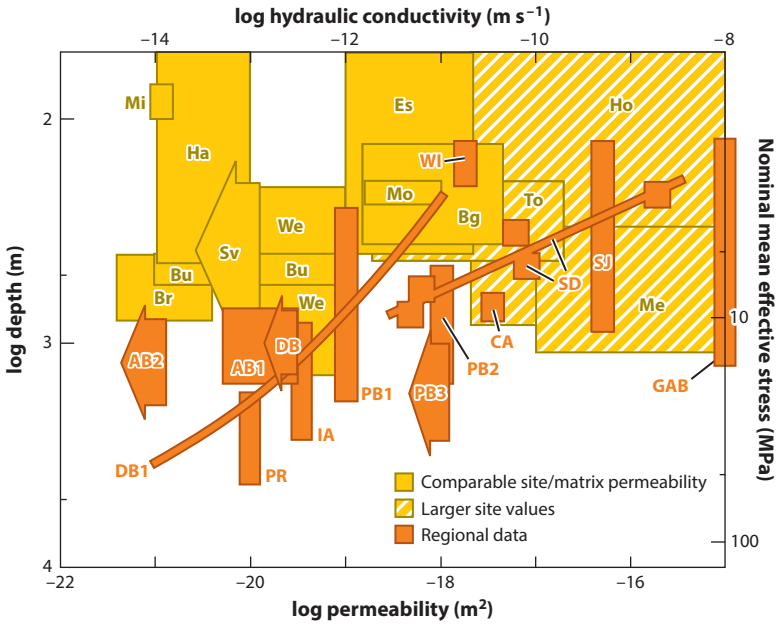


**Bg** Oligocene to Miocene clay, Burgos, Spain: ~0.02 km²

**Br** Paleozoic shales, Bruce County, Ontario, Canada: ~4 km²

**Bu** Jurassic argillite, Bure, France: ~3 km²

**Es** Cretaceous shales, Esterhazy, Saskatchewan, Canada: ~0.1 km²

**Ha** Cretaceous shale, Hayes, South Dakota, USA: ~0.1 km²

**Ho** Miocene siliceous mudstone, Horonobe, Japan: ~8 km²

**Me** Paleozoic claystone, Mecsek, Hungary: ~0.3 km²

**Mi** Paleozoic shale near Milwaukee, Wisconsin, USA: ~30 km²

**Mo** Oligocene clay, Mol, Belgium: ~0.2 km²

**Sv** Mesozoic shales and siltstones, Adventdalen, Svalbard: ~4 km²

**To** Jurassic marl and argillite, Tournemire, France: ~1 km²

**We** Cretaceous and Tertiary marl and argillaceous marl, Wellenberg, Switzerland: ~4 km²

**AB1** Cretaceous shales, Alberta Basin, Canada: ~30,000 km²

**AB2** Cretaceous shales, Alberta Basin, Canada: ~400,000 km²

**DB, DB1** Cretaceous shales, Denver Basin, USA as single value and depth trend: ~160,000 km²

**GAB** Cretaceous mudstones, Great Artesian Basin, Australia: ~1,000,000 km²

**IA, CA** Paleozoic shales, Illinois–Appalachian Basin and Cincinnati Arch, USA: ~400,000 km²

**PB1** Triassic, Jurassic, and Cretaceous confining units, Paris Basin, France: ~200,000 km²

**PB2, PB3** Jurassic and Cretaceous confining units, and Triassic and Jurassic confining units, Paris Basin, France: ~200,000 km²

**PR** Cretaceous shales, Powder River Basin, USA: ~50,000 km²

**SD** Cretaceous shales, South Dakota, USA: ~160,000 km²

**SJ** Cretaceous shales, San Juan Basin, USA: ~5,000 km²

**WI** Paleozoic shale, Wisconsin, USA: ~7,000 km²

**Figure 7**

Site- and regional-scale permeability of clay and shale formations in continent interiors versus depth. The hydraulic conductivity scale is for aqueous fluids at room temperature. Site data in yellow for areas of $10^{-2}$ to $10^{2}$ km² are from Neuzil (2015) and sources therein unless otherwise noted; solid yellow indicates site and matrix permeability values are comparable, while patterned yellow indicates site values are larger. Regional data for areas of $10^{3}$ to $10^{6}$ km² in orange are from the sources noted. Areas listed are the approximate extent of each formation in which the permeability shown is thought to apply. Arrows indicate values that are maxima due to model nonuniqueness. AB1 data are from Corbet & Bethke (1992), AB2 data are from Bekele (1999), CA data are from Gupta & Bair (1997), DB (single value) and DB1 (depth trend) data are from Belitz & Bredehoeft (1988), GAB data are from Bethke et al. (1999), IA data are from Gupta & Bair (1997), Mi data are from Eaton et al. (2007), PB1 data are from Wei et al. (1990), PB2 and PB3 data are from Castro et al. (1998), PR data are from McPherson et al. (2001), SD data are from Bredehoeft et al. (1983), SJ data are from Phillips et al. (1989), Sv data are from Wangen et al. (2015), and WI data are from Hart et al. (2006).

Available data fall naturally into two scale classes in **Figure 7**, namely regional permeabilities (areas of $10^{3}$ to $10^{6}$ km²) and site permeabilities (areas of $10^{-2}$ to $10^{2}$ km²). The latter include data already presented in **Figure 5** and are based on both inverse analyses and extensive laboratory and borehole testing at well-studied locations, some of which host underground laboratories. Regional data derive from flow across argillaceous strata and so are strongly controlled by the lowest permeability horizons within those sequences. Some data in **Figure 7** are maxima due to

model nonuniqueness. In the Denver Basin, for example, Belitz & Bredehoeft (1988) found that all shale permeability values less than about $3 \times 10^{-20}$ m$^2$, including zero, could explain aquifer behavior equally well.

Scale effects are conspicuous in both site and regional data in **Figure 7**. Where site-scale permeability is larger than matrix values from the same formation, borehole testing and other evidence indicate the presence of numerous conductive fractures, the influence of which is also seen in **Figure 4**. Formations at the sites in question (Tournemire, France; Mecsek, Hungary; and Horonobe, Japan) are distinguished by low mineralogical clay fractions (recall that mudstone at Horonobe is mostly clay-sized silica). As discussed in Section 2.3, this may explain the presence of transmissive fractures (Bourg 2015).

Regional permeabilities tend to be larger than most site values at depths less than about 1 km. This implies the features that increase permeability are often sufficiently localized to be absent at many sites. Disparity between regional and site values is less apparent and may be absent at depths exceeding about 1 km as regional permeabilities approach laboratory matrix values for low porosities. This is consistent with certain other observations; fractures in the Barnett Shale, for example, are reportedly closed or sealed at depths of 1.5 to 2.5 km (Bowker 2007) despite it having a relatively low clay fraction. Effective stress may thus be an important control of regional permeability at these depths, but the possibility that we are instead seeing anthropogenic effects is considered at the end of the next section.

### 3.3. Dynamic Permeability and Scale Effects

It has long been understood that permeability evolves with geologic systems over long periods of time as exemplified by permeability decreases in sediments as they compact and undergo diagenesis (e.g., **Figure 3**; Section 2.2). However, there is growing recognition that permeability in the crust changes, or is dynamic, on a range of timescales (Manga et al. 2012, Ingebritsen & Gleeson 2015) as a variety of phenomena enhance and decrease it (Ingebritsen & Manning 2010). This more current notion of dynamic permeability has particular significance in the present context because large-scale permeability values represent behavior integrated over time spans that are long in human terms. Dynamic permeability in clays and shales also has important practical implications, notably with respect to waste isolation and protection of groundwater resources.

Dynamic permeability entered the discussion in Section 3.1 when considering episodic fluid releases that limit fluid pressures on continental margins. In fact, several lines of evidence point to periods of increased flow through argillaceous sediments on both convergent and passive margins. In the Gulf of Mexico these include apparent oil migration across shales (Finkbeiner et al. 2001) and salinity, temperature, and pressure anomalies thought to reflect episodic fluid expulsion from shales (Roberts et al. 1996). Salinity and temperature patterns in the Barbados accretionary complex and faulting in argillaceous sequences in the North Sea have also been linked to cyclical changes in permeability (Cartwright 1994, Bekins et al. 1995).

We have seen that large-scale permeabilities from inverse analyses in margin environments differ little from matrix permeabilities (**Figure 5**; Section 3.1). Because these time-integrated values apparently incorporate episodes of increased permeability, the increases must be relatively limited in magnitude or, as is more likely, duration. Simulations of temperature and pressure patterns observed by Roberts et al. (1996) support this conclusion, suggesting expulsion events lasting just tens of years in the Gulf Coast. In the Barbados accretionary complex, salinity patterns analyzed by Bekins et al. (1995) were consistent with episodes in which décollement permeability abruptly increases by two to three orders of magnitude for $10^2$ to $10^3$ years. Multiple lines of

evidence indicate that regions of increased fluid pressure and permeability in décollements are local in extent and migrate (Brown et al. 1994, Saffer 2015).

Dynamic permeability presents greater challenges in continent interiors because of their varied and often complex geologic histories. The pervasiveness of fractures and faults indicates that most clays and shales may at some time have experienced permeability increases followed by decreases where these features are now closed or mineral filled (Constantin et al. 2004). Evolving tectonic stress regimes presumably are responsible for much of the fracturing, faulting, and reactivation of these features (e.g., Engelder 1993), although some may have been caused by high fluid pressures in deep basins (e.g., McPherson & Bredehoeft 2001) or even glaciation (Neuzil 2011).

At depths less than 1 km, fracture-enhanced permeability appears limited to lithologies with low mineralogical clay fractions (Tournemire, France; Mt. Terri, Switzerland; and Horonobe, Japan, in **Figure 4**, noting that the Horonobe, Japan, lithology is mostly clay-sized silica). This is consistent with observations that clay and shale fractures created in damage zones around underground excavations and in laboratory experiments self-seal on decadal or shorter timescales, apparently by viscoelastic deformation and swelling of clays in addition to mineral precipitation (Bock et al. 2010). Likewise, the lack of distinct scale effects in regional permeability at depths exceeding about 1 km (**Figure 7**; Section 3.2) implies that any permeability increases there, if they occur, are also relatively small or short-lived. Regional-scale permeabilities in the uppermost kilometer, however, are a different matter; features responsible for differences between regional and site permeabilities, and the extent to which they are dynamic, are largely unknown (see Section 5).

Seismic shaking is the only natural phenomenon linked by direct observations to permeability increases in argillaceous formations. Increased streamflow and aquifer connectivity across clay confining units occurred after the 1999 Chi-Chi earthquake in Taiwan. Wang et al. (2016) concluded that shaking opened or unclogged fractures in clay confining units and shales, increasing vertical permeability more than a hundredfold to depths of several kilometers. Increases in vertical permeability in mudstone and shale to several kilometers of depth were also reported by Liao et al. (2015) and Shi & Wang (2016) in the Sichuan Basin, China, following the 2008 Wenchuan earthquake. Because these areas are seismically active, permeabilities apparently return to low values on timescales shorter than the recurrence interval of major earthquakes or, in the Taiwan case, over hundreds of years at most. Effects of the Wenchuan earthquake were noted at epicentral distances exceeding 400 km, suggesting that such permeability changes can be extensive.

Human activities compose a distinct class of dynamic permeability mechanisms. Fluid injection–induced seismicity, for example, often appears to enhance permeability generally (Ingebritsen & Manning 2010), and argillaceous caprocks may hydrofracture when injection raises fluid pressure (e.g., White et al. 2014). However, abandoned and poorly sealed wells may cause the most pervasive and widespread changes in clay and shale confining layers and caprocks. Abandoned oil and gas exploration and production wells in interior basins in North America likely number in the tens of thousands, many of which probably leak (Nordbotten et al. 2004). Abandoned water-supply wells tend to be shallower but more numerous, with more than 50,000 estimated to exist in the US state of South Dakota alone (SD Dep. Environ. Nat. Resour. 2018), an average of one every 4 $km^2$. Leaky wells can profoundly alter how clay and shale formations control regional flow. For example, the regional permeability of the Paleozoic Maquoketa Shale (**Figure 7**) is about $10^3$ times greater than its matrix permeability, and Hart et al. (2006) calculated that just 50 leaking wells at spacings of 10 km could account for the difference. The influence of leaking wells is consistent with the observation that regional scale effects decrease with depth and largely disappear below 1 km depth.

## 4. CLAY AND SHALE PERMEABILITY IN CONTEXT

Many nonargillaceous lithologies, notably crystalline rocks, fine-grained carbonate and silicate sedimentary rocks, and evaporites, also have quite low matrix permeabilities (Trimmer et al. 1980, Beauheim & Roberts 2002, Mallon et al. 2005, Kurikame et al. 2008). Except for evaporites, however, these lithologies are nearly always fractured and relatively permeable over scales of meters to tens of meters and greater (e.g., Freeze & Cherry 1979). Zoback & Townend (2001) noted that near-hydrostatic fluid pressures detected by deep boreholes signal that permeabilities no smaller than about $10^{-17}$ m$^2$ are commonly present to 10–12 km depths. This is broadly consistent with borehole test data compilations (Ranjram et al. 2015) as well as estimates based on geothermal constraints and mass transport required during metamorphism (Manning & Ingebritsen 1999).

Permeability estimates for sizable volumes of nonargillaceous lithologies in continent interiors are rare, but the few that are available probably offer the most meaningful direct comparison for the clay and shale data presented in **Figure 7**. Such a comparison is shown in **Figure 8** with depth now on a linear scale. Data height and width again show ranges of depth and permeability.

At depths to 1 km, site permeabilities (areas of $10^{-2}$ to $10^{2}$ km$^2$) for clays and shales are as much as eight orders of magnitude smaller than the other lithologies shown. For depths to about 5 km, regional permeabilities (areas of $10^{3}$ to $10^{6}$ km$^2$) for shales suggest that permeability decreases with depth at a fractional rate similar to other lithologies but at values some four to five orders of magnitude lower. This stark contrast may persist to greater depths if permeabilities of $10^{-17}$ m$^2$ do in fact extend to 10–12 km in most lithologies as Zoback & Townend (2001) suggested.

Clay-rich sequences often are identifiable and apparently continuous over distances of $10^{3}$ km or more in continent interiors as, for example, in the Rocky Mountain foreland and the Western Siberia Basin (e.g., Mossop & Shetsen 1994, Vyssotski et al. 2006). Due to this sheet-like geometry at regional scales, **Figure 8** implies that clay and shale formations impart a megascale regional permeability architecture that is distinctly anisotropic, strongly limits vertical flow and transport, and caps underlying basement rocks. Because site and regional clay and shale permeabilities often differ in the uppermost 1 km, vertical flow and transport in sedimentary terrains at these depths may typically be focused in discrete locations such as zones of fracturing, faults, or other discontinuities in clay and shale strata as discussed in the next section.

## 5. DISCUSSION AND CHALLENGES

Developing a picture of clay and shale permeability and its scale dependence in different geological settings is possible by synthesizing laboratory testing, in situ characterization, and, most crucially, inverse modeling of flow systems at large scales. Extensive laboratory and in situ test data are now available, thanks partly to the emergence of scientific ocean drilling and nuclear waste programs as prolific contributors of high-quality data. Inverse model analysis, however, has been underutilized for investigating permeability at the largest scales. Although the discovery that many shallow intraplate clay and shale formations are anomalously pressured has spurred recent inverse analyses at many sites (Neuzil 2013, 2015), little attention is currently focused on analyzing regional flow systems for this purpose. Unfortunately, many regional groundwater systems may be sufficiently altered by fluid extraction, injection, and leaky boreholes that analysis is now problematic (e.g., see Hart et al. 2006, Eaton et al. 2007).

Data that are available allow several generalizations. Clay and shale matrix permeability shows a consistent trend of decrease with porosity despite the complex mix of compaction, diagenesis, decompaction, and retrograde diagenesis represented in the data (**Figure 3**). Clay-rich sediments in major river deltas on passive continental margins and in accretionary complexes on convergent

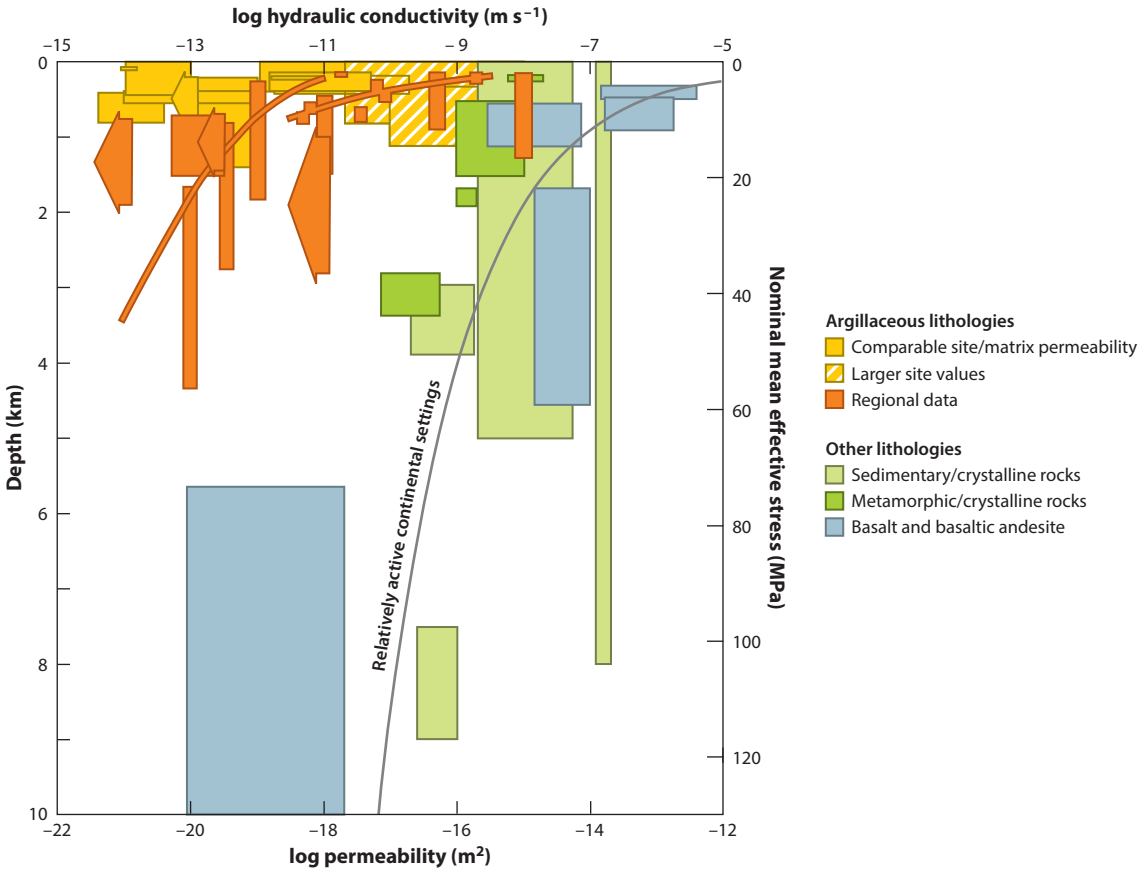


**Figure 8**

Permeability with depth of large volumes of argillaceous and other lithologies and the brittle continental crust generally. The hydraulic conductivity scale is for aqueous fluids at room temperature. Yellow and orange are site ($10^{-2}$–$10^{2}$ km$^2$) and regional ($10^{3}$–$10^{6}$ km$^2$) clay and shale data as in **Figure 7**, light and dark green are sedimentary/crystalline rocks and metamorphic/crystalline rocks (Townend & Zoback 2000), blue is basalt and basaltic andesite (Saar & Manga 2004), and the gray curve represents relatively active continental settings and is constrained by heat transport (Ingebritsen & Manning 1999). Data for nonargillaceous rocks were derived from seismicity triggered by human-caused fluid pressure changes that occurred on short timescales, often weeks or months, whereas the clay and shale data and active crust curve represent behavior integrated over periods of time that are long in human terms.

margins are natural laboratories showing this behavior and appear to be the most voluminous low-permeability regions anywhere in the shallow crust, reaching thicknesses in excess of 10 km over areas of $10^4$ to $10^5$ km$^2$ (Laske & Masters 2018, Nat. Ocean. Atmos. Admin. 2018). Although overpressured fluids apparently escape episodically along fractures and faults in these dynamic environments, available estimates of their time-integrated large-scale permeability differ little from matrix values (**Figure 5**). This is consistent with independent evidence that fluid expulsion occurs as short-lived, local permeability increases that migrate (Roberts et al. 1996, Saffer 2015).

In continent interiors, inverse model analyses of anomalously pressured clay and shale formations and regional flow systems reveal seemingly systematic relations between permeability and scale (**Figure 7**). At depths less than about 1 km, regional (areas of $10^3$ to $10^6$ km$^2$) vertical permeabilities of clay and shale formations tend to be larger than matrix values, often by several orders of magnitude. When specific sites (areas of $10^{-2}$ to $10^2$ km$^2$) are investigated, however, increased

permeability due to fracturing appears limited to clays and shales with relatively low porosities and clay contents. Otherwise, clay and shale formations generally appear to have site permeabilities comparable to matrix values. Together, these observations suggest that regional permeabilities are controlled by leakage at discrete locations.

The features that enhance permeability at the regional scale are largely a mystery. Because fractures in most clays and shales appear to close relatively quickly even at shallow depths (Bock et al. 2010), faults and fault zones may seem to be likely culprits. However, the effects of faults on fluid flow are complex and generalizations difficult. In most lithologies evidence suggests that faults behave as conduit-barrier systems in which flow is enhanced in the fault plane and impeded across it (Bense et al. 2013), but faults in most clays and shales may not transmit any significant flow (Clennell et al. 1998). Argillaceous media sheared in the laboratory to emulate faulting, for example, have shown permeability decreases (Brown et al. 1994), while in situ testing has revealed minimal permeability increases in faults in Jurassic claystone in Switzerland (Yu et al. 2017). Faults in some argillaceous formations, however, do show evidence of cycles of increased and decreased fluid transmission during tectonism (Constantin et al. 2004). Faults can also offset clay and shale strata, connecting over- and underlying permeable strata.

In addition to tectonic faults, polygonal fault systems of uncertain origin have been identified in clays and shales on continental margins and interiors (Cartwright et al. 2003, Szmigielski & Hendry 2017). Other features known to disrupt clay and shale strata include collapse structures above evaporite and carbonate karst (Johnson 1997, Szmigielski & Hendry 2017), blowout structures linked to Pleistocene subglacial recharge (Grasby et al. 2000), and even buried bolide impact structures (Sawatzky 1977). From a regional perspective, sedimentary terrains may be peppered with such features. For example, Szmigielski & Hendry (2017) found that shale strata were disrupted by two to ten collapse structures per 100 $km^2$ in the part of the Williston Basin they studied.

Characterization of clay and shale permeability at the largest scales is made uncertain in general by inherent limitations of inverse analysis and in particular by unanswered questions about flow behavior in clay aggregates. Although rarely recognized as such, large-scale flow in clays and shales is entirely inferential because it cannot be observed directly. Pressure anomalies, for example, are analyzed as transient Darcian flow (Neuzil 1995) (see the sidebar titled Fluid Pressure Anomalies and Permeability), but the presumed flow and pressure evolution are far too slow to observe (Mase & Smith 1987). And, while transient flow in clays and shales can be observed in the laboratory, such tests require hydraulic gradients orders of magnitude greater than in nature (Section 2.1). Thus, inverse analyses are based on extrapolations from artificially large hydraulic gradients and behavior in much more permeable materials.

This observational gap might be of little concern if not for theoretical considerations and experimental studies some have interpreted as indicative of non-Darcian behavior in clay aggregates, usually in the form of reduced or no flow at low hydraulic gradients (see the sidebar titled Non-Darcian and Coupled Flow in Argillaceous Materials). Coupled flows such as chemical osmosis that occur in clays and shales (Mitchell 1993) further complicate matters. If coupled flows are significant, Darcy's law offers an incomplete, if correct, description. These uncertainties affect treatment of problems that range from waste isolation to understanding the presence of pressure anomalies in old basins (e.g., Lee & Deming 2002).

Improving experimental techniques sufficiently to resolve these questions seems unlikely because achieving the necessary thermal, mechanical, and flow stability in tests is quite challenging. An alternative approach, through analyzing fundamental physical and chemical phenomena controlling fluid flow through clay nanopores, is receiving increasing attention as numerical computation capabilities increase. Molecular dynamics (MD) simulations are beginning to enable studies of

changes in fluid properties near solid surfaces, the usual conceptual underpinning of non-Darcian behavior, with some MD simulation efforts already examining whether flow in clay nanopores produces Darcian macroscopic behavior (Boţan et al. 2011, Bourg & Steefel 2012).

## DISCLOSURE STATEMENT

The author has received funding from the Canadian Nuclear Waste Management Organization.

## ACKNOWLEDGMENTS

This work was supported by the National Research Program of the US Geological Survey. I am grateful to Barbara Bekins and an anonymous reviewer for insightful comments on the manuscript.



## LITERATURE CITED

Anandarajah A. 2003. Mechanism controlling permeability change in clays due to changes in pore fluid. *J. Geotech. Geoenvironmental Eng.* 129:163–72

Beauheim RL, Roberts RM. 2002. Hydrology and hydraulic properties of a bedded evaporite formation. *J. Hydrol.* 259:66–88

Beauheim RL, Roberts RM, Avis JD. 2014. Hydraulic testing of low-permeability Silurian and Ordovician strata, Michigan Basin, southwestern Ontario. *J. Hydrol.* 509:163–78

Bekele EB. 1999. *Anomalous pressures and fluid migration within the Alberta Basin, Canada*. PhD Thesis, Univ. Minn., Minneapolis

Bekins BA, Matmon D, Screaton EJ, Brown KM. 2011. Reanalysis of in situ permeability measurements in the Barbados décollement. *Geofluids* 11:57–70

Bekins BA, McCaffrey AM, Dreiss SJ. 1995. Episodic and constant flow models for the origin of low-chloride waters in a modern accretionary complex. *Water Resour. Res.* 31:3205–15

Belitz K, Bredehoeft JD. 1988. Hydrodynamics of Denver basin: explanation of subnormal fluid pressures. *AAPG Bull.* 72:1334–59

Bense VF, Gleeson T, Loveless SE, Bour O, Scibek J. 2013. Fault zone hydrogeology. *Earth-Sci. Rev.* 127:171–92

Best ME, Katsube TJ. 1995. Shale permeability and its significance in hydrocarbon exploration. *Leading Edge* 14:165–70

Bethke CM. 1986. Inverse hydrologic analysis of the distribution and origin of Gulf Coast-type geopressured zones. *J. Geophys. Res.* 91(B6):6535–45

Bethke CM, Zhao X, Torgersen T. 1999. Groundwater flow and the $^{4}$He distribution in the Great Artesian Basin of Australia. *J. Geophys. Res.* 104(B6):12999–3011

Bjørlykke K. 1998. Clay mineral diagenesis in sedimentary basins—a key to the prediction of rock properties. Examples from the North Sea Basin. *Clay Miner.* 33:15–34

Bock H, Dehandschutter B, Martin CD, Mazurek M, de Haller A, et al. 2010. *Self-sealing of fracture in argillaceous formations in the context of geological disposal of radioactive waste, review and synthesis*. NEA Rep. 6164, Nuclear Energy Agency, Paris

Boisson J-Y, ed. 2005. *Clay Club Catalogue of Characteristics of Argillaceous Rocks*. Paris: OECD Publ.

Boisson J-Y, Bertrand L, Heitz J-F, Moreau-Le Golvan Y. 2001. In situ and laboratory investigations of fluid flow through an argillaceous formation at different scales of space and time, Tournemire tunnel, southern France. *Hydrogeol. J.* 9:108–23

Bossart P, Bernier F, Birkholzer J, Bruggeman C, Connolly P, et al. 2017. Mont Terri rock laboratory, 20 years of research: introduction, site characteristics and overview of experiments. *Swiss J. Geosci.* 110:3–22

Boţan A, Rotenberg B, Marry V, Turq P, Noetinger B. 2011. Hydrodynamics in clay nanopores. *J. Phys. Chem. C* 115:16109–15

Boulin PF, Bretonnier P, Gland N, Lombard JM. 2010. *Low water permeability measurements of clay sample. Contribution of steady state method compared to transient methods*. Paper presented at the International Symposium of the Society of Core Analysts, Halifax, N.S., Oct. 4–7

Bourg IC. 2015. Sealing shales versus brittle shales: a sharp threshold in the material properties and energy technology uses of fine-grained sedimentary rocks. *Environ. Sci. Technol. Lett.* 2:255–59

Bourg IC, Steefel CI. 2012. Molecular dynamics simulations of water structure and diffusion in silica nanopores. *J. Phys. Chem. C* 116:11556–64

Bowker KA. 2007. Barnett Shale gas production, Fort Worth Basin: issues and discussion. *AAPG Bull.* 91:523–33

Brasier FW, Kobelski BJ. 1996. Injection of industrial wastes in the United States. In *Deep Injection Disposal of Hazardous and Industrial Waste, Scientific and Engineering Aspects*, ed. JA Apps, C-F Tsang, pp. 1–8. New York: Academic

Bredehoeft J. 2005. The conceptualization model problem—surprise. *Hydrogeol. J.* 13:37–46

Bredehoeft JD, Neuzil CE, Milly PCD. 1983. *Regional flow in the Dakota aquifer: a study of the role of confining layers*. US Geol. Surv. Water Supply Pap. 2237, US Geol. Surv., Reston, VA

Brown KM, Bekins B, Clennell B, Dewhurst D, Westbrook G. 1994. Heterogeneous hydrofracture development and accretionary fault dynamics. *Geology* 22:259–62

Bryant WR. 2002. Permeability of clays, silty-clays and clayey-silts. *Gulf Coast Assoc. Geol. Soc. Trans.* 52:1069–77

Cartwright JA. 1994. Episodic basin-wide hydrofracturing of overpressured Early Cenozoic mudrock sequences in the North Sea Basin. *Mar. Pet. Geol.* 11:587–607

Cartwright JA, James D, Bolton A. 2003. The genesis of polygonal fault systems: a review. In *Subsurface Sediment Mobilization*, ed. P Van Rensbergen, RR Hillis, AJ Maltman, CK Morely, pp. 223–43. London: Geol. Soc.

Castro MC, Goblet P, Ledoux E, Violette S, de Marsily G. 1998. Noble gases as natural tracers of water circulation in the Paris Basin 2. Calibration of a groundwater flow model using noble gas isotope data. *Water Resour. Res.* 34:2467–83

Clennell MB, Dewhurst DN, Brown KM, Westbrook GK. 1999. Permeability anisotropy of consolidated clays. In *Muds and Mudstones: Physical and Fluid-Flow Properties*, ed. AC Aplin, AJ Fleet, JHS Macquaker, pp. 79–96. London: Geol. Soc.

Clennell MB, Knipe RJ, Fisher QJ. 1998. Fault zones as barriers to, or conduits for, fluid flow in argillaceous formations: a microstructural and petrophysical perspective. In *Fluid Flow Through Faults and Fractures in Argillaceous Formations, Proceedings of a Joint NEA/EC Workshop, Berne, Switzerland, 10–12 June, 1996*, pp. 125–39. Paris: OECD Publ.

Constantin J, Peyaud JB, Vergély P, Pagel M, Cabrera J. 2004. Evolution of the structural fault permeability in argillaceous rocks in a polyphased tectonic context. *Phys. Chem. Earth* 29:25–41

Corbet TF, Bethke CH. 1992. Disequilibrium fluid pressures and groundwater flow in the Western Canada Sedimentary Basin. *J. Geophys. Res.* 97(B5):7203–17

Croisé J, Schlickenrieder L, Marschall P, Boisson J-Y, Vogel P, Yamamoto S. 2004. Hydrogeological investigations in a low permeability claystone formation: the Mont Terri Rock Laboratory. *Phys. Chem. Earth* 29:3–15

Daigle H, Screaton EJ. 2015. Evolution of sediment permeability during burial and subduction. *Geofluids* 15:84–105

Davis EE, Horel GC, MacDonald RD, Villinger H, Bennett RH, Li H. 1991. Pore pressures and permeabilities measured in marine sediments with a tethered probe. *J. Geophys. Res.* 96(B4):5975–84

Delay J, Trouiller A, Lavanchy J-M. 2006. Propriétés hydrodynamiques du Callovo-Oxfordien dans l'Est du bassin de Paris: comparaison des résultats obtenus selon différentes approches. *C. R. Geosci.* 338:892–907

Dewhurst DN, Aplin AC, Sarda J-P. 1999. Influence of clay fraction on pore-sale properties and hydraulic conductivity of experimentally compacted mudstones. *J. Geophys. Res.* 104(B12):29261–74

Dixon DA, Graham J, Gray MN. 1999. Hydraulic conductivity of clays in confined tests under low hydraulic gradients. *Can. Geotech. J.* 36:815–25

Dugan B, Flemings PB. 2000. Overpressure and fluid flow in the New Jersey continental slope: implications for slope failure and cold seeps. *Science* 289:288–91

Dugan B, Sheahan TC. 2012. Offshore sediment overpressures of passive margins: mechanisms, measurement, and models. *Rev. Geophys.* 50:RG3001

Eaton TT, Anderson MP, Bradbury KR. 2007. Fracture control of ground water flow and water chemistry in a rock aquitard. *Ground Water* 45:601–15

Engelder T. 1993. *Stress Regimes in the Lithosphere*. Princeton, NJ: Princeton Univ. Press

Fertl WH. 1976. *Abnormal Formation Pressures*. Amsterdam: Elsevier

Finkbeiner T, Zoback M, Flemings P, Stump B. 2001. Stress, pore pressure, and dynamically constrained hydrocarbon columns in the South Eugen Island 330 field, northern Gulf of Mexico. *AAPG Bull.* 85:1007–31

Fisher AT, Zwart G. 1997. Packer experiments along the decollement of the Barbados accretionary complex: measurements of in situ permeability. In *Proceedings of the Ocean Drilling Program Scientific Results*, Vol. 156, ed. TH Shipley, Y Ogawa, P Blum, JM Bahr, pp. 199–218. College Station, TX: Ocean Drill. Program

Freeze RA, Cherry JA. 1979. *Groundwater*. Englewood Cliffs, NJ: Prentice-Hall

Gamage K, Screaton E, Bekins B, Aiello I. 2011. Permeability-porosity relations of subduction zone sediments. *Mar. Geol.* 279:19–36

Giot R, Giraud A, Auvray C. 2014. Assessing the permeability in anisotropic and weakly permeable porous rocks using radial pulse tests. *Oil Gas Sci. Technol Rev. IFP Energ. Nouv.* 69:1171–89

Gonçalvès J, Violette S, Wendling J. 2004. Analytical and numerical solutions for alternative overpressuring processes: application to the Callovo-Oxfordian sedimentary sequence in the Paris basin, France. *J. Geophys. Res.* 109:B02110

Grasby S, Osadetz K, Betcher R, Render F. 2000. Reversal of the regional-scale flow system of the Williston Basin in response to Pleistocene glaciation. *Geology* 28:635–38

Gupta N, Bair ES. 1997. Variable-density flow in the midcontinent basins and arches region of the United States. *Water Resour. Res.* 33:1785–802

Harrison WJ, Summa LL. 1991. Paleohydrology of the Gulf of Mexico Basin. *Am. J. Sci.* 291:109–76

Hart DJ, Bradbury KR, Feinstein DT. 2006. The vertical hydraulic conductivity of an aquitard at two spatial scales. *Ground Water* 44:201–11

Heitzmann P, ed. 2004. *Mont Terri Project—Hydrogeological Synthesis, Osmotic Flow*. Bern, Ger.: Bundesamt Wasser Geol.

Horsrud P, Sønstebø EF, Bøe R. 1998. Mechanical and petrophysical properties of North Sea shales. *Int. J. Rock Mech. Min. Sci.* 35:1009–20

Ingebritsen SE, Gleeson T. 2015. Crustal permeability: introduction to the special issue. *Geofluids* 15:1–10

Ingebritsen SE, Manning CE. 1999. Geological implications of a permeability-depth curve for the continental crust. *Geology* 27:1107–10

Ingebritsen SE, Manning CE. 2010. Permeability of the continental crust: dynamic variations inferred from seismicity and metamorphism. *Geofluids* 10:193–205

Ingebritsen SE, Sanford WE, Neuzil CE. 2006. *Groundwater in Geologic Processes*. Cambridge, UK: Cambridge Univ. Press

Intera Eng. Ltd. 2011. *Descriptive Geosphere Site Model*. Toronto: Intera Eng. Ltd.

Intergov. Panel Clim. Change. 2005. *Carbon Dioxide Capture and Storage*, ed. B Metz, O Davidson, H de Coninck, M Loos, L Meyer. New York: Cambridge Univ. Press

Johnson KS. 1997. Evaporite karst in the United States. *Carbonates Evaporites* 12:2–4

Katsube TJ, Williamson MA. 1994. Effects of diagenesis on shale nano-pore structure and implications for sealing capacity. *Clay Miner.* 29:451–61

Katsuki D, Gutierrez M, Tutuncu AN. 2014. *Improved constant rate of strain consolidation test on stiff shale*. Paper presented at the Unconventional Resources Technology Conference, Denver, CO, Aug. 25–27

Kitajima H, Chester FM, Biscontin G. 2012. Mechanical and hydraulic properties of Nankai accretionary prism sediments: effect of stress path. *Geochem. Geophys. Geosyst.* 13:Q0AD27

Koltermann CE, Gorelick SM. 1995. Fractional packing model for hydraulic conductivity derived from sediment mixtures. *Water Resour. Res.* 31:3283–97

Kufner S-K, Hüpers A, Kopf AJ. 2014. Constraints on fluid flow processes in the Hellenic Accretionary Complex (eastern Mediterranean Sea) from numerical modeling. *J. Geophys. Res. Solid Earth* 119:3601–26

Kurikame H, Takeuchi R, Yabuuchi S. 2008. Scale effect and heterogeneity of hydraulic conductivity of sedimentary rocks at Horonobe URL site. *Phys. Chem. Earth* 33:S37–44

Kwon O, Kronenberg AK, Gangi AF, Johnson B, Herbert BE. 2004. Permeability of illite-bearing shale: 1. Anisotropy and effects of clay content and loading. *J. Geophys. Res.* 109(B10):B10205

Laske G, Masters G. 2018. *A global digital map of sediment thickness*. Map, 1 × 1° scale, Univ. Calif., San Diego. **http://igppweb.ucsd.edu/~gabi/sediment.html#ftp**

Lecampion B, Constantinescu A, Malinsky L. 2006. Identification of poroelastic constants of "tight" rocks from laboratory tests. *Int. J. Geomech.* 6:201–8

Lee Y, Deming D. 2002. Overpressures in the Anadarko basin, southwestern Oklahoma: static or dynamic? *AAPG Bull.* 86:145–60

Liao X, Wang C-Y, Liu C-P. 2015. Disruption of groundwater systems by earthquakes. *Geophys. Res. Lett.* 42:9758–63

Liu H-H, Li L, Birkholzer J. 2012. Unsaturated properties for non-Darcian water flow in clay. *J. Hydrol.* 430–31:173–78

Luijendijk E, Gleeson T. 2015. How well can we predict permeability in sedimentary basins? Deriving and evaluating porosity-permeability equations for noncemented sand and clay mixtures. *Geofluids* 15:67–83

Mallon AJ, Swarbrick RE, Katsube TJ. 2005. Permeability of fine-grained rocks: new evidence from chalks. *Geology* 33:21–24

Manga M, Beresnev I, Brodsky EE, Elkhoury JE, Elsworth D, et al. 2012. Changes in permeability caused by transient stresses: field observations, experiments, and mechanisms. *Rev. Geophys.* 50:RG2004

Manning CE, Ingebritsen SE. 1999. Permeability of the continental crust: implications of geothermal data and metamorphic systems. *Rev. Geophys.* 37:127–50

Mase CW, Smith L. 1987. The role of pore fluids in tectonic processes. *Rev. Geophys.* 25:1348–58

McPherson BJOL, Bredehoeft JD. 2001. Overpressures in the Uinta basin, Utah: analysis using a three-dimensional basin evolution model. *Water Resour. Res.* 37:857–91

McPherson BJOL, Lichtner PC, Forster CB, Cole BS. 2001. Regional-scale permeability by heat flow calibration in the Powder River Basin, Wyoming. *Geophys. Res. Lett.* 28:3211–14

Mesri G, Olson RE. 1971. Mechanisms controlling the permeability of clays. *Clays Clay Miner.* 19:151–58

Mitchell JK. 1993. *Fundamentals of Soil Behavior*. New York: Wiley. 2nd ed.

Moore JC, Shipley TH, Goldberg D, Ogawa Y, Filice F, et al. 1995. Abnormal fluid pressures and fault-zone dilation in the Barbados accretionary prism: evidence from logging while drilling. *Geology* 23:605–8

Mossop GD, Shetsen I, eds. 1994. *Geological Atlas of the Western Canada Sedimentary Basin*. Calgary: Can. Soc. Pet. Geol.

Natl. Ocean. Atmos. Admin. 2018. *Total sediment thickness of the world's oceans and marginal seas, version 2*. Data Sheet, Natl. Ocean. Atmos. Admin., Washington, DC. **http://www.ngdc.noaa.gov/mgg/sedthick/**

Natl. Genoss. Lager. Radioakt. Abfälle. 2002. *Projekt Opalinuston, Synthese der geowissenschaftlichen Untersuchungsergebnisse*. NAGRA Tech. Bericht NTB 02-03, Natl. Genoss. Lager. Radioakt. Abfälle, Wettingen, Switz.

Neuzil CE. 1986. Groundwater flow in low-permeability environments. *Water Resour. Res.* 22:1163–95

Neuzil CE. 1993. Low fluid pressure within the Pierre Shale: a transient response to erosion. *Water Resour. Res.* 29:2007–20

Neuzil CE. 1994. How permeable are clays and shales? *Water Resour. Res.* 30:145–50

Neuzil CE. 1995. Abnormal pressures as hydrodynamic phenomena. *Am. J. Sci.* 295:742–86

Neuzil CE. 2011. Hydromechanical effects of continental glaciation on groundwater systems. *Geofluids* 12:22–37

Neuzil CE. 2013. Can shale safely host U.S. nuclear waste? *Eos Trans. AGU* 94:261–62

Neuzil CE. 2015. Interpreting fluid pressure anomalies in shallow intraplate argillaceous formations. *Geophys. Res. Lett.* 42:4801–8

Neuzil CE, Provost AM. 2009. Recent experimental data may point to a greater role for osmotic pressures in the subsurface. *Water Resour. Res.* 45:W03410

Nordbotten JM, Celia MA, Bachu S. 2004. Analytical solutions for leakage rates through abandoned wells. *Water Resour. Res.* 40:W04204

Ota K, Abe H, Yamaguchi T, Kunimaru T, Ishii E, et al. 2007. *Horonobe Underground Research Laboratory Project, synthesis of phase I investigations 2001–2004, volume "Geoscientific Research."* JAEA-Research 2007-044, Jpn. At. Energy Agency, Ibaraki, Jpn.

Parker BL, Cherry JA, Chapman SW. 2004. Field study of TCE diffusion profiles below DNAPL to assess aquitard integrity. *J. Contam. Hydrol.* 74:197–230

Phillips FM, Tansey MK, Peeters LA, Cheng S, Long A. 1989. An isotopic investigation of groundwater in the central San Juan Basin, New Mexico: carbon 14 dating as a basis for numerical flow modeling. *Water Resour. Res.* 25:2259–73

Pickens JF, Grisak GE, Avis JD, Belanger DW, Thury M. 1987. Analysis and interpretation of borehole hydraulic tests in deep boreholes: principles, model development, and applications. *Water Resour. Res.* 23:1341–75

Potter PE, Maynard JB, Depetris PJ. 2005. *Mud and Mudstones: Introduction and Overview*. New York: Springer

Ranjram M, Gleeson T, Luijendijk E. 2015. Is the permeability of crystalline rock in the shallow crust related to depth, lithology or tectonic setting? *Geofluids* 15:106–19

Reece JS, Flemings PB, Dugan B, Long H, Germaine JT. 2012. Permeability-porosity relationships of shallow mudstones in the Ursa Basin, northern deepwater Gulf of Mexico. *J. Geophys. Res.* 117:B12102

Reisdorf AG, Hostettler B, Jaeggi D, Deplazes G, Bläsi H, et al. 2016. *Litho- and biostratigraphy of the 250 m-deep Mont Terri BDB-1 borehole through the Opalinus Clay and bounding formations, St-Ursanne, Switzerland*. Rep., Mont Terri Proj., Swiss Geol. Surv., Wabern, Switz.

Revil A, Grauls D, Brévart O. 2002. Mechanical compaction of sand/clay mixtures. *J. Geophys. Res.* 107(B11):2293

Roberts R, Chace D, Beauheim R, Avis J. 2011. *Analysis of straddle-packer tests in DGR boreholes*. Tech. Rep. TR-08-32, Geofirma Eng. Ltd, Ottawa, Can.

Roberts SJ, Nunn JA, Cathles L, Cipriani F-D. 1996. Expulsion of abnormally pressured fluids along faults. *J. Geophys. Res.* 101(B12):28231–52

Saar MO, Manga M. 2004. Depth dependence of permeability in the Oregon Cascades inferred from hydrogeologic, thermal, seismic, and magmatic modeling constraints. *J. Geophys. Res.* 109:B04204

Saffer DM. 2015. The permeability of active subduction plate boundary faults. *Geofluids* 15:193–215

Saffer DM, Bekins BA. 1998. Episodic flow in the Nankai accretionary complex: timescale, geochemistry, flow rates, and fluid budget. *J. Geophys. Res.* 103(B12):30351–70

Saffer DM, Bekins BA. 2006. An evaluation of factors influencing pore pressure in accretionary complexes: implications for taper angle and wedge mechanics. *J. Geophys. Res.* 111:B04101

Saffer DM, Tobin HJ. 2011. Hydrogeology and mechanics of subduction zone forearcs: fluid flow and pore pressure. *Annu. Rev. Earth Planet. Sci.* 39:157–86

Sanada H, Niunoya S, Matsui H, Fujii Y. 2009. Influences of sedimentary history on the mechanical properties and microscopic structure change of Horonobe siliceous rocks. *J. Min. Mater. Process. Inst. Jpn.* 125:521–29

Sawatzky HB. 1977. Buried impact craters in the Williston Basin and adjacent area. In *Impact and Explosion Cratering*, ed. DJ Roddy, RO Pepin, RB Merrill, pp. 461–80. New York: Pergamon

Schlömer S, Krooss BM. 1997. Experimental characterization of the hydrocarbon sealing efficiency of cap rocks. *Mar. Pet. Geol.* 14:565–80

Schneider J, Flemings PB, Day-Stirrat RJ, Germaine JT. 2011. Insights into pore-scale controls on mudstone permeability through resedimentation experiments. *Geology* 39:1011–14

SD Dep. Environ. Nat. Resour. 2018. *Abandoned wells in South Dakota*. Rep., SD Dep. Environ. Nat. Resour., Pierre. **http://denr.sd.gov/des/wr/abandonedwell.aspx**

Shi Z, Wang G. 2016. Aquifers switched from confined to semiconfined by earthquakes. *Geophys. Res. Lett.* 43:11166–72

Smerdon BD, Smith LA, Harrington GA, Gardner WP, Delle Piane C, Sarout J. 2014. Estimating the hydraulic properties of an aquitard from in situ pore pressure measurements. *Hydrogeol. J.* 22:1875–87

Spinelli GA, Giambalvo ER, Fisher AT. 2004. Sediment permeability, distribution, and influence on fluxes in oceanic basement. In *Hydrogeology of the Oceanic Lithosphere*, ed. EE Davis, H Elderfield, pp. 151–88. Cambridge, UK: Cambridge Univ. Press

Stack AG. 2015. Precipitation in pores: a geochemical frontier. *Rev. Mineral. Geochem.* 80:165–90

Szmigielski JT, Hendry MJ. 2017. Secondary rock structures and the regional hydrogeology of claystone-rich Cretaceous strata, Williston Basin, Saskatchewan, Canada. *Can. J. Earth Sci.* 54:902–18

Tachi Y, Yotsuji K, Seida Y, Yui M. 2011. Diffusion and sorption of $Cs^+$, $I^-$ and HTO in samples of the argillaceous Wakkanai Formation from the Horonobe URL, Japan: clay-based modeling approach. *Geochem. Cosmochem. Acta* 75:6742–59

Thyberg B, Jahren J, Winje T, Bjørlykke K, Faleide JI, Marcussen Ø. 2010. Quartz cementation in Late Cretaceous mudstones, northern North Sea: changes in rock properties due to dissolution of smectite and precipitation of micro-quartz crystals. *Mar. Pet. Geol.* 27:1752–64

Townend J, Zoback MD. 2000. How faulting keeps the crust strong. *Geology* 28:399–402

Trimmer D, Bonner B, Heard HC, Duba A. 1980. Effect of pressure and stress on water transport in intact and fractured gabbro and granite. *J. Geophys. Res.* 85(B12):7059–71

US Energy Inf. Admin. 2015. *World shale resource assessments*. Rep., US Energy Inf. Admin., Washington, DC. **https://www.eia.gov/analysis/studies/worldshalegas/**

van der Kamp G. 2001. Methods for determining the in situ hydraulic conductivity of shallow aquitards—an overview. *Hydrogeol. J.* 9:5–16

Vinard P, Bobet A, Einstein HH. 2001. Generation and evolution of hydraulic underpressures at Wellenberg, Switzerland. *J. Geophys. Res.* 106(B12):30593–605

Vinsot A, Delay J, de la Vaissière R, Cruchaudet M. 2011. Pumping tests in a low permeability rock: results and interpretation of a four-year long monitoring of water production flow rates in the Callovo-Oxfordian argillaceous rock. *Phys. Chem. Earth* 36:1679–87

Vyssotski AV, Vyssotski VN, Nezhdanov AA. 2006. Evolution of the West Siberian Basin. *Mar. Pet. Geol.* 23:93–126

Walsh R. 2011. *Compilation and consolidation of field and laboratory data for hydrogeological properties*. DGR Site Charact. Doc. Geofirma Eng. Proj. 08-200, TR-08-10, Geofirma Eng. Ltd., Ottawa, Can.

Wang C-Y, Liao X, Wang L-P, Wang C-H, Manga M. 2016. Large earthquakes create vertical permeability by breaching aquitards. *Water Resour. Res.* 52:5923–37

Wangen M, Souche A, Johansen H. 2015. A model for underpressure development in a glacial valley, an example from Adventdalen, Svalbard. *Basin Res.* 28:752–69

Wei HF, Ledoux E, de Marsily G. 1990. Regional modelling of groundwater flow and salt and environmental tracer transport in deep aquifers in the Paris Basin. *J. Hydrol.* 120:341–58

Westbrook GK, Smith MJ. 1983. Long decollements and mud volcanoes: evidence from the Barbados Ridge Complex for the role of high pore-fluid pressure in the development of an accretionary complex. *Geology* 11:279–83

White JA, Chiaramonte L, Ezzedine S, Foxall W, Hao Y, et al. 2014. Geomechanical behavior of the reservoir and caprock system at the Salah $CO_2$ storage project. *PNAS* 111:8747–52

Winkler KW. 2005. Borehole damage indicator from stress-induced velocity variations. *Geophysics* 70:F11–16

Wood LJ. 2010. Shale tectonics: a preface. In *Shale Tectonics*, ed. LJ Wood, pp. 1–4. Tulsa: Am. Assoc. Pet. Geol.

Yang Y, Aplin AC. 2007. Permeability and petrophysical properties of 30 natural mudstones. *J. Geophys. Res.* 112:B03206

Yang Y, Aplin AC. 2010. A permeability-porosity relationship for mudstones. *Mar. Pet. Geol.* 27:1692–97

Yu C, Matray J-M, Gonçalvès J, Jaeggi D, Gräsle W, et al. 2017. Comparative study of methods to estimate hydraulic parameters in the hydraulically undisturbed Opalinus Clay (Switzerland). *Swiss J. Geosci.* 110:85–104

Yu L, Rogiers B, Gedeon M, Marivoet J, De Craen M, Mallants D. 2013. A critical review of laboratory and in-situ hydraulic conductivity measurements for the Boom Clay in Belgium. *Appl. Clay Sci.* 75–76:1–12

Yven B, Sammartino S, Géraud Y, Homand F, Villiéras F. 2007. Mineralogy, texture and porosity of Callovo-Oxfordian argillites of the Meuse/Haute-Marne region (eastern Paris Basin). *Mém. Soc. Géol. Fr.* 178:73–90

Zhang J, Scherer GW. 2012. Permeability of shale by the beam-bending method. *Int. J. Rock Mech. Min. Sci.* 53:179–91

Zhang M, Takahashi M, Morin RH, Endo H, Esaki T. 2002. Determining the hydraulic properties of saturated, low-permeability geological materials in the laboratory: advances in theory and practice. In *Evaluation and Remediation of Low Permeability and Dual Porosity Environments*, ed. MN Sara, LG Everett, pp. 83–98. West Conshohocken, PA: ASTM Int.

Zoback MD, Townend J. 2001. Implications of hydrostatic pore pressure and high crustal strength for the deformation of intraplate lithosphere. *Tectonophysics* 336:19–30

Zwart G, Brukmann W, Moran K, MacKillop AK, Maltman AJ, et al. 1997. Evaluation of hydrogeologic properties of the Barbados accretionary prism: a synthesis of Leg 156 results. In *Proceedings of the Ocean Drilling Program Scientific Results*, Vol. 156, ed. TH Shipley, Y Ogawa, P Blum, JM Bahr, pp. 303–10. College Station, TX: Ocean Drill. Program